



**Politecnico
di Torino**

Abstract of Master Thesis in Mechanical Engineering:
**“Development of a MATLAB code for 3D-dynamic simulation
of multi-span ropeway systems”**

Supervisor:

Prof. Luigi Garibaldi

Student:

Mojtaba Ahani

Date:

December 2021

1 Contents

1 Contents	2
2 Introduction.....	4
2.1 Cable transport systems and State of art	4
2.2 Work organization.....	6
2.3 Literature review	7
3 Modelling and Simulation approach.....	9
3.1 Introduction to the adopted Finite element approach and formulation	9
3.1.1 Euler-Bernoulli element and formulation (G.Genta, 2008).....	9
3.1.2 Effect of axial force on flexural behavior.....	21
3.2 Time Integration: Newmark Scheme for dynamic study	23
4 1 st Configuration: Single-Span cable	25
4.1 Implementation of Euler-Bernoulli beam element.....	25
4.1.1 Global behavior of the beam	25
4.1.2 From local to global reference frame and rotation matrices.....	27
4.1.3 Assembling and mapping matrices.....	29
4.2 Boundary Conditions and Static equilibrium.....	32
4.2.1 Calculation of Static equilibrium and Reaction Forces	34
4.3 Modal analysis of the system and validation	37
4.4 Dynamic responses of the system	40
4.4.1 Step Response.....	41
4.4.2 Harmonic Response.....	43
4.4.3 Response to moving load.....	45
5 2 nd Configuration: Multi-Span cable.....	49
5.1 Implementation of E-B element,.....	49
5.1.1 From local to global reference frame and rotation matrices.....	49
5.1.2 Assembling and mapping matrices.....	52
5.2 Boundary Conditions and Static equilibrium.....	53
5.2.1 Calculation of Static equilibrium and Reaction Forces	55
5.3 Modal analysis of the system and validation	57

5.4 Dynamic responses of the system	62
5.4.1 Step Response.....	62
5.4.2 Harmonic Response.....	64
5.4.3 Response to moving load.....	65
5.5 Sensitivity to the length of element.....	67
6 3 rd Configuration: Multi-Span beam carrying multiple lumped elements and a lumped system	69
6.1 Introducing lumped elements to the system.....	70
6.2 Introducing lumped system (dynamic shock absorber) to the system	72
6.3 Results	73
7 Conclusion	75
Acknowledgement	76
List of figures.....	77
List of tables.....	79
Bibliography	80

2 Introduction

2.1 Cable transport systems and State of art

Cable Transport is a wide means of transportation characterized by one or more cables. They often utilize vehicles called cable cars to transport passengers and goods while the cable may be of different types driven or passive. A cable car (U.K., Europe), similarly called an aerial lift (U.S.), is one type of cable transport mechanism that hauls cabins, cars, gondolas, or open chairs above the ground through several cables. Aerial lift systems have been extensively adopted in places where building roads are not convenient such as mountainous territories and even mining sites. Unfortunately, despite maximum care, which is being taken within their missions, there are still accidents happening every year. Although some of them are due to human mistakes, yet a great deal of them occurs owing to a combination of poor engineering design and operational conditions.

A gondola lift is a type of cable car which is made up of only one wire rope generally of steel material. The cable is circulated and strung between two stations and usually passing over multiple intermediate-supporting towers. An engine or electric motor is utilized to drive the cable with a constant line speed through a bull wheel in a terminal to provide propulsion within the operation.



Figure 2-1 _ Gondola lift

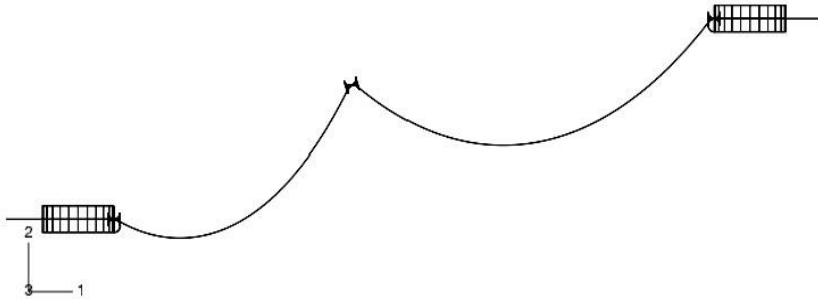


Figure 2-2 _ An illustrative 3D model of a gondola lift with two spans

Another kind of cable car is a ropeway (even known as an aerial tramway, sky tram, or aerial tram), characterized by using one or two stationary ropes (track cables) as supports for passenger or cargo cabins. These cabins are rigidly connected to a set of wheels named the truck rolling on the track cables. Additionally, another moving rope is implemented so that provides propulsion (haulage rope). Within this type of system, an aerial tramway cabin's grip is fixed onto the haulage rope that is driven by an electric motor throughout the operation.



Figure 2-3 _ Aerial Tramway

In a gondola lift, moving cable carries loads and masses fixed to the cable itself and according to previous work, it can be analyzed as a fixed cable subjected to moving loads and masses with minor and negligible error. Speaking of ropeways, ignoring the interaction of moving rope on the track cable (stationary one), which is a negligible effect, we can adopt the same consideration to study the behavior of the track cable. In conclusion, our simulation holds for the two system configurations.

The cable in gondola lifts and the track cables in ropeways are subjected to various loading conditions in both vertical (parallel to the field of gravity) and lateral direction (orthogonal to the field of gravity) such as the weight of multiple moving mass in the vertical and wind in the lateral direction. Each one of these loadings may contribute to severe conditions that eventually end up in strand fatigue failure usually taking place at points where the cable motion is constrained against transverse vibration, such as at suspensions and boundaries. As a result, it is necessary to analyze the dynamic behavior of the system under these

situations. Owing to difficulties in operating measurements on the field, studying the system dynamic response mostly relies on numerical analysis.

Since there are not many published works in this regard, this work is dedicated to deal with the above issues and address the challenges we face when simulating the track cable. The main objective that concerns this work is initially developing FE-code in MATLAB to perform a three-dimensional simulation of a multi-span beam as a (track) cable having each span with different lengths and orientations in space. In this case, the system has been discretized by adopting a 1D Euler-Bernoulli beam element. Euler-Bernoulli beam element has two nodes on which the inertia, damping, and stiffness properties are lumped, and six degrees of freedom are associated with each node. Afterward, having a global mass matrix and global stiffness matrix of the entire structure, modal analysis of the system was carried out to extract the mode shapes associated with the first five smallest natural frequencies of the system which can be considered as the most important ones among the others.

2.2 Work organization

Validation of the developed MATLAB model is an essential step to proceed with this project's remaining tasks, which mainly involves analysis of the dynamic behavior of the system. Consequently, validation has been carried out firstly by using commercial FEM software (ABAQUS) to perform modal analysis. Within ABAQUS simulation, the B33 element type was adopted which represents quadratic E-B beam element in space. Subsequently, further assessment of the MATLAB FE-model accomplished through successfully generating the correct results and mode shapes for a multi-span Euler-Bernoulli beam carrying several various concentrated elements including point masses, rotary inertias, linear springs, rotational springs, and spring-mass systems. This system is investigated in a paper.

To study the dynamic behavior of the system, initially, as the real system is subjected to various loadings, it is necessary to analyze a different kind of forced responses of the system. Accordingly, step response, harmonic response, and the response of the system to multiple moving loads and even multiple moving masses have been investigated in the current work, in which the latter represents several cargo cabins passing through the (track) cable in the vertical plane. On the other side, wind pressure over the moving cabins has been studied which simply means excitation in the lateral plane. In order to perform these analyses, the Newmark algorithm has been adopted in this work, which is an implicit time integration scheme to discretize second-order time systems and widely used for structural dynamic analysis.

2.3 Literature review

The study of oscillation and dynamic behavior of the ropes during operation in cable car systems is a topic that has not been developed in detail. The companies working on this area, have not considered it essential developing dynamic simulation on the entire line as the study of the static configuration has always been, to calculate the necessary values of the design.

However, before starting the study, research has been carried out on previous literature relevant to the topics on which our analysis is to be developed. With respect to ropeway dynamics, there are only a few texts available that mostly cover the wind effects on the cable and cabins. Some articles dedicated to these arguments are as the following:

- (Zhou Yang, Xue-Ping Li, Jun Li, Tian-Sheng Hong, Kun-Peng Xue, 2015)
- (R.Petrova, St.Karapetkov, S.Dechkova, Pl.Petrov, 2011)
- (K.Hoffmann, R.Petrova, 2009)

In thesis work (Sciuto, 2015) in order to characterize the dynamic behavior of the system in critical conditions, an on-line dynamic analysis for an aerial cable car system was carried out with a focus on the vibrations of the cabins, adopting GNSS methodologies (Global Navigation Satellite System) and GPS / INS (Inertial System).

Also, a lot of information has been found regarding the vibrations of ropes in the railway sector (catenary-pantograph system) and even vibrations in overhead energy transmission lines. On the latter there is much innovative research dedicated to the damping of oscillations, for example in the study (BUSCEMI, 2016) with the translated title "Study of an active control system for the reduction of vibrations in overhead electricity transmission lines", and in the thesis work by Onore (2018), whose translated title is "Stockbridge damper and vibration suppression of thesis cables: numerical and experimental analysis". With respect to ropeway systems used for transporting people, there are many texts and guidelines that refer to the study and design of the line, including for example the textbook (A. Crotti, 2006) in which, however, there are no dynamic aspects. Given the scarcity of papers and literature regarding the oscillations of the ropes, focused precisely on the cableway systems, it is therefore decided to undertake a complete study of the dynamics of ropeway systems.

Furthermore, the work (B. Carboni, A. Arena, W. Lacarbonara, 2020) is dedicated to developing a passive vibration control strategy to reduce peak accelerations on the roller conveyors. In this analysis the damping system tries to reduce the vertical accelerations of the vehicles. The study of the oscillations that is addressed in the thesis (Belluati, 2021) in addition to the analysis of the carrier oscillations, concerns the analysis of the spring system applied to the rope, trying to confirm or deny the hypothesis that the damping system can lead to an attenuation of the oscillations on the haul rope (thus obtaining an increase in the damping factor).

With respect to catenary-pantograph systems, there are valuable works and papers available. For instance, a comprehensive overview was performed in the study of interaction problems in catenary-pantograph systems in the work (G. Poetsch, J. Evans, 1997). This work is dedicated to the assessment of different

approaches to analyze and to verify the dynamic behavior of the catenary and pantograph system as well as aspects of acquisition data for the model. Regarding the model describing the dynamics of catenary, as far as the bending stiffness of the rope is a key factor within the high-frequency range of interaction, adopting beam models (in this case, negligible variation among Timoshenko and Euler-Bernoulli beam), these result more reliable if compared to string model. As numerical solutions to the catenary differential equation, there are three different methods assessed in this study: modal analysis which suffers from lack of flexibility with respect to structural design, D'Alembert's traveling wave approach which despite its exceptional reliability, in this case, is based on string model in one dimension.-Then Finite Element Method (FEM) and Finite Difference Method (FDM), which provides a high degree of flexibility but also costly in terms of computation time. Additionally, in (D. Anastasio, A. Fasana, L. Garibaldi, S. Marchesiello, 14 June 2018), a further investigation on the experimental validation for the analytical method are performed to introduce a trustworthy dynamic model for the overhead contact line. In this study, the wire is modeled adopting a homogeneous Euler-Bernoulli beam element under tensile load, accompanied by lumped elastic and inertial elements.

In the dissertation (Anastasio, 2020 May 14), conducted at Politecnico di Torino, robust techniques are developed for nonlinear vibrating structures, by identifying nonlinear characteristics of real structures based on the nonlinear subspace identification (NSI) method by implementing custom finite element formulation. Eventually, the presented method is applicable in the railway arena, especially to study the interaction problems in catenary-pantograph systems. Moreover, in this work, attention is paid toward the enhancement of the system performance by designing ad-hoc nonlinear damping.

Regarding the static equilibrium assessment, which is another important aspect to analyze, in the work (O.Lopez-Garcia, A.Carniceroa, V.Torresb, 2006) an accurate method is introduced for railway overheads to calculate static configuration and stiffness distribution according to the catenary equation. Furthermore, in (Yong Hyeon Cho, Kiwon Lee, 2010) study of static equilibrium was carried out by taking advantage of both analytical and FEM formulations.

Some relevant research projects have been conducted at the Technical University of Lisbon regarding a finite element formulation for the catenary, listed below:

- (Rauter, 2007)
- (Ambrósio, 2012)
- (J.Pombo, J.Ambrósio, 2012 a)
- (J.Pombo, J.Ambrósio , 2012 b)
- (J.Pombo, J.Ambrosio, 2013)

In addition, to consider also the lateral oscillation of the cable, an advanced 3D model has been developed in (H.Sugiyama & Ahmed A. Shabana, 2005), (Ning Zhou, 2011), (J.-H. Lee and T.-W. Park., 2012), (J. Benet et al., 2013). These models introduced the capability of considering side wind excitation on the cable.

3 Modelling and Simulation approach

The finite element method has been utilized in this work which is one of the most widely adopted techniques to discretize systems. The possibility of adopting this approach for a vast variety of problems, and in addition to that and more importantly, the increasing power of the available computing machines, has made this method reliable and more successful. Usually, the systems modeled using this method end up with a large number (hundreds, thousands, or even millions) of degrees of freedom. Although, for general purposes, the obtained ordinary differential equations are easily implemented in codes for digital computers and can be used both in time-domain and frequency-domain computations.

3.1 Introduction to the adopted Finite element approach and formulation

3.1.1 Euler-Bernoulli element and formulation (G.Genta, 2008)

Among different approaches in finite element, the beam element is one of the most frequently adopted elements and is available in all software and computer codes. There are numbers of beam formulations developed which differ based on the number of nodes and degrees of freedom on each element and the theoretical formulation.

Euler-Bernoulli element is a prismatic homogeneous beam that does not consider the shear deformation and has been utilized in this work. In 3D configuration, a two-node element including six degrees of freedom (DOF) per node is considered, in which the DOFs are namely, axial displacement u_z , transverse displacement in x-direction u_x , transverse displacement in y-direction u_y , and rotations θ_z, θ_x , and θ_y respectively about z, x, and y axes, ending up with 12 DOFs per element. The nodal displacement vector will be:

$$\{q\} = \{u_{z1} \ u_{x1} \ u_{y1} \ \theta_{z1} \ \theta_{x1} \ \theta_{y1} \ u_{z2} \ u_{x2} \ u_{y2} \ \theta_{z2} \ \theta_{x2} \ \theta_{y2}\}'_{1 \times 12}$$

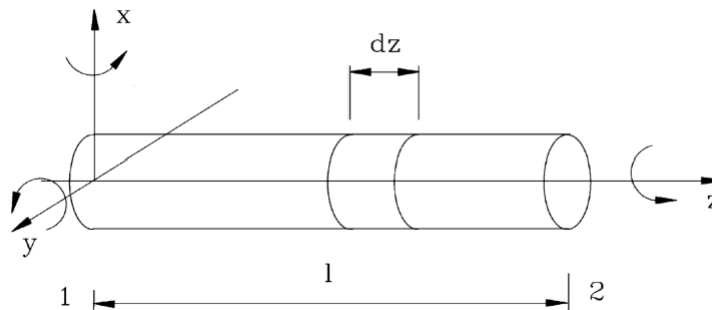


Figure 3-1 _ Beam element and reference frame

The displacement of points inside the element is calculated by the following equation:

$$u(x, y, z, t) = N(x, y, z)q(t) \quad (3.1)$$

In which, $q(t)$ is the vector containing generalized coordinates of the elements (the nodal displacement vector) and $N(x, y, z)$ is the shape function matrix.

Since the strains of the element are functions of displacement derivative with respect to space coordinate, the expression could be written as:

$$\epsilon(x, y, z, t) = B(x, y, z)q(t) \quad (3.2)$$

where $\epsilon(x, y, z, t)$ is column vector including the elements of the strain tensor and elements inside matrix $B(x, y, z)$ are appropriate derivatives of the corresponding elements in shape function matrix.

For an element, free from initial stresses and strains, and inside the linear range of material behavior, the relationship between stresses and strains is:

$$\sigma(x, y, z, t) = \mathbf{E}\epsilon = \mathbf{E}(x, y, z)B(x, y, z)q(t) \quad (3.3)$$

Where $\mathbf{E}(x, y, z)$, stiffness matrix of the material, is a square symmetric matrix and its elements are usually constant through the element but theoretically are functions of space coordinate.

From the potential energy expression, one can be written:

$$\mathcal{U} = \frac{1}{2} \int \epsilon^T \sigma dV = \frac{1}{2} q^T \left(\int B^T \mathbf{E} B dV \right) q \quad (3.4)$$

From eq (3.4), the stiffness matrix of the element can be expressed as:

$$K = \int B^T \mathbf{E} B dV \quad (3.5)$$

Since in eq (3.1), the only time dependent variable is $q(t)$, the generalized velocity is:

$$\dot{u}(x, y, z, t) = N(x, y, z)\dot{q}(t) \quad (3.6)$$

From the expression of the kinetic energy, the mass matrix of the element can be easily derived:

$$\mathcal{T} = \frac{1}{2} \int \rho \dot{u}^T \dot{u} dV = \frac{1}{2} \dot{q} \left(\int \rho N^T N dV \right) \dot{q},$$

$$M = \int \rho N^T N dV \quad (3.7)$$

in which ρ is the density of the material.

In the presence of a distributed force $f(x, y, z, t)$ acting on the element, the link between virtual work and virtual displacement is:

$$\begin{aligned} \delta u &= N \delta q, \\ \delta \mathcal{L} &= \int \delta u^T f(x, y, z, t) dV = \int \delta q^T N^T f(x, y, z, t) dV \end{aligned}$$

Then the nodal force vector can be expressed as:

$$f(t) = \int N^T f(x, y, z, t) dV \quad (3.8)$$

Due to the properties of the beam, un-coupling between different behavior of the beam (axial, torsional, and flexural) is feasible. Hence, subdividing the vector \mathbf{q} into four smaller ones:

$$\{q_A\} = \begin{Bmatrix} u_{z1} \\ u_{z2} \end{Bmatrix}, \quad \{q_T\} = \begin{Bmatrix} \theta_{z1} \\ \theta_{z2} \end{Bmatrix}, \quad \{q_{F1}\} = \begin{Bmatrix} u_{x1} \\ \theta_{y1} \\ u_{x2} \\ \theta_{y2} \end{Bmatrix}, \quad \{q_{F2}\} = \begin{Bmatrix} u_{y1} \\ \theta_{x1} \\ u_{y2} \\ \theta_{x2} \end{Bmatrix}$$

By reordering the coordinates, vector \mathbf{q} can be written as:

$$\{q\} = \{q_A^T \quad q_T^T \quad q_{F1}^T \quad q_{F2}^T\}^T$$

The uncoupling provides the possibility to split the shape function matrix into a number of submatrices in the form of a diagonal matrix (eq 3.9). Subsequently, calculations for each behavior will be possible to perform individually. For an internal point of the element, the generalized coordinates could be expressed as:

$$u(z, t) = \begin{Bmatrix} u_z \\ \theta_z \\ u_x \\ \theta_y \\ u_y \\ \theta_x \end{Bmatrix} = \begin{bmatrix} N_A & 0 & 0 & 0 \\ 0 & N_T & 0 & 0 \\ 0 & 0 & N_{F1} & 0 \\ 0 & 0 & 0 & N_{F2} \end{bmatrix} \begin{Bmatrix} q_A \\ q_T \\ q_{F1} \\ q_{F2} \end{Bmatrix} \quad (3.9)$$

Axial behavior – z direction

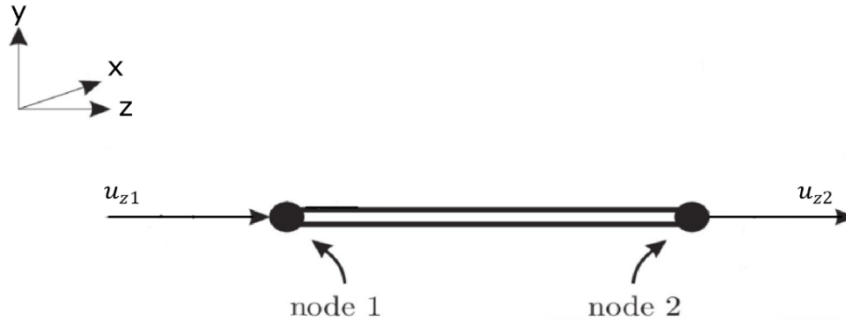


Figure 3-2 _ Euler-Bernoulli beam element and axial degrees of freedom

In this special case, one considers the beam as a bar with only axial strain as the only degree of freedom at each node along the z -axis (u_z), and the nodal displacement vector q_A has two rows and one column. Either the shape function matrix N_A corresponding to the axial behavior is a matrix of one row and two columns (there are only two DOFs in the element).

$$\{q_A\} = \begin{Bmatrix} u_{z1} \\ u_{z2} \end{Bmatrix} \quad N_A = [1 - \zeta \quad \zeta]$$

which $\zeta = z/l$, and l is the length of element.

Here the vector ϵ has one element which is the axial strain ϵ_z :

$$\epsilon_z = \frac{du_z}{dz} = \left[\frac{d}{dz} (1 - \zeta) \quad \frac{d}{dz} \zeta \right] \begin{Bmatrix} u_{z1} \\ u_{z2} \end{Bmatrix},$$

and matrix B is:

$$B = \left[\frac{d}{dz} (1 - \zeta) \quad \frac{d}{dz} \zeta \right] = \frac{1}{l} [-1 \quad 1] \quad (3.10)$$

Either the vector σ and the matrix E are of only one element which respectively is axial stress σ_z and the Young's modulus E .

From Eqs (3.5) and (3.7), the stiffness and mass matrices of the element in the axial behavior can easily be obtained as follows:

$$K_A = \int_0^l AB^T EB dz = \frac{EA}{l} \begin{bmatrix} 1 & -1 \\ -1 & 1 \end{bmatrix} \quad (3.11)$$

$$M_A = \int_0^l \rho AN^T N dz = \frac{\rho Al}{6} \begin{bmatrix} 2 & 1 \\ 1 & 2 \end{bmatrix} \quad (3.12)$$

In the presence of a distributed axial load $f_z(t)$ that is constant along z , or concentrated axial load $F_{z_k}(t)$ located on z_k , acting on the bar, the nodal force vector can be expressed as:

$$f(t) = l \left[\int_0^l \begin{Bmatrix} (1-\zeta) \\ \zeta \end{Bmatrix} d\zeta \right] f_z(t) = f_z(t) \frac{l}{2} \begin{Bmatrix} 1 \\ 1 \end{Bmatrix}, \quad (3.13)$$

or

$$f(t) = F_{z_k}(t) \begin{Bmatrix} 1 - \frac{z_k}{l} \\ \frac{z_k}{l} \end{Bmatrix}, \quad (3.14)$$

Torsional behavior

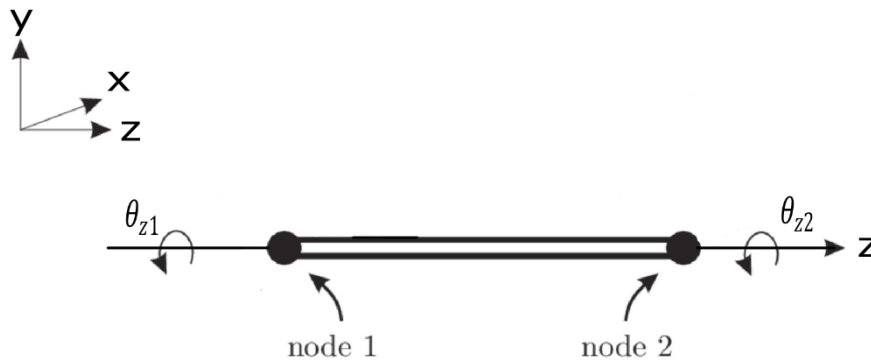


Figure 3-3 _ Euler-Bernoulli beam element and torsional degrees of freedom

As for axial behavior, the equation of motion concerning the torsional behavior of the Euler-Bernoulli element is identical to that of axial behavior; except for the fact that the degrees of freedom, in this case,

is rotation in z axis (θ_z). The shape function matrix N_T and the nodal displacement vector q_T are either of the same dimension:

$$\{q_T\} = \begin{Bmatrix} \theta_{z1} \\ \theta_{z2} \end{Bmatrix} \qquad N_T = [1 - \zeta \quad \zeta]$$

where $\zeta = z/l$, and l is the length of element.

And the expressions for the matrices are:

$$K_T = \frac{GI_p'}{l} \begin{bmatrix} 1 & -1 \\ -1 & 1 \end{bmatrix} \qquad (3.15)$$

$$M_T = \frac{\rho I_p l}{6} \begin{bmatrix} 2 & 1 \\ 1 & 2 \end{bmatrix} \qquad (3.16)$$

Where $I_p [m^4]$ is the polar moment of inertia and $I_p' [m^4]$ is the torsional moment of inertia, which due to circular cross-section, both values coincide with each other. The expression $G [\frac{N}{m^2}]$ represents shear modulus.

Flexural behavior – xz plane

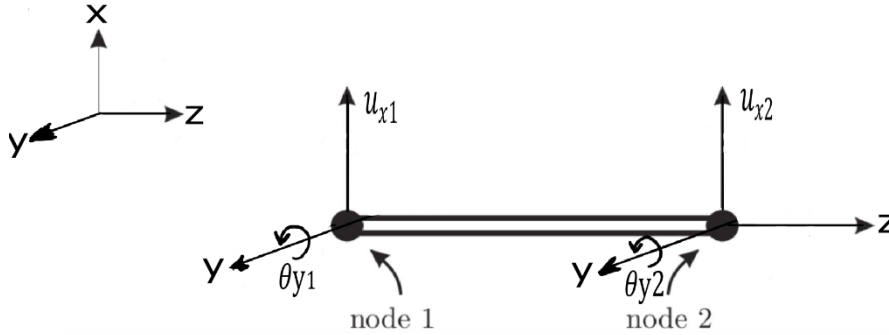


Figure 3-4 _ Euler-Bernoulli beam element and flexural degrees of freedom within xz plane

To each node are associated two DOFs, a translational one along the x axis (u_x) and a rotational one around the y axis (θ_y). This means that the mass and stiffness matrices associated to this discretized element have a 4×4 size.

According to the Euler Bernoulli approach for the slender beams, the rotation of each cross-section can be expressed with the derivative of the displacement. Hence, the polynomial expressions for the generalized displacements of the element are:

$$\begin{cases} u_x(z) = \alpha_1 + \alpha_2 z + \alpha_3 z^2 + \alpha_4 z^3 \\ \theta_y(z) = \frac{\partial u_x(z)}{\partial z} = \alpha_2 + 2\alpha_3 z + 3\alpha_4 z^2 \end{cases} \quad (3.17)$$

Rewriting Eq (3.17):

$$\begin{Bmatrix} u_x \\ \theta_y \end{Bmatrix} = \begin{bmatrix} 1 & z & z^2 & z^3 \\ 0 & 1 & 2z & 3z^2 \end{bmatrix} \begin{Bmatrix} \alpha_1 \\ \alpha_2 \\ \alpha_3 \\ \alpha_4 \end{Bmatrix} = [\Phi(z)]\{\alpha\} \quad (3.18)$$

To link the displacement of the element with the nodal displacements:

$$\begin{cases} u_x(0) = \alpha_1 \\ \theta_y(0) = \alpha_2 \\ u_x(l) = \alpha_1 + \alpha_2 l + \alpha_3 l^2 + \alpha_4 l^3 \\ \theta_y(l) = \alpha_2 + 2\alpha_3 l + 3\alpha_4 l^2 \end{cases}$$

It can be rearranged as:

$$\{q_{F1}\} = \begin{Bmatrix} u_{x1} \\ \theta_{y1} \\ u_{x2} \\ \theta_{y2} \end{Bmatrix} = \begin{bmatrix} 1 & 0 & 0 & 0 \\ 0 & 1 & 0 & 0 \\ 1 & l & l^2 & l^3 \\ 0 & 1 & 2l & 3l^2 \end{bmatrix} \begin{Bmatrix} \alpha_1 \\ \alpha_2 \\ \alpha_3 \\ \alpha_4 \end{Bmatrix} = [A]\{\alpha\} \quad (3.19)$$

From Eqs (3.18) and (3.19), it can be written as:

$$\begin{Bmatrix} u_x \\ \theta_y \end{Bmatrix} = [\Phi(z)][A]^{-1}\{q_{F1}\} = [N_{F1}]\{q_{F1}\}$$

in this case, the shape function matrix N_{F1} and the nodal displacement vector q_{F1} are as the following:

$$\{q_{F1}\} = \{u_{x1} \ \theta_{y1} \ u_{x2} \ \theta_{y2}\}'_{1 \times 4} \quad N_{F1} = \begin{bmatrix} N_{11} & N_{12} & N_{13} & N_{14} \\ N_{21} & N_{22} & N_{23} & N_{24} \end{bmatrix}$$

Where:

$$\begin{aligned} N_{11} &= 1 - 3\zeta^2 + 2\zeta^3 & N_{21} &= \frac{6\zeta}{l}(\zeta - 1) \\ N_{12} &= l\zeta(1 - 2\zeta + \zeta^2) & N_{22} &= (1 - 4\zeta + 3\zeta^2) \\ N_{13} &= \zeta(3\zeta - 2\zeta^2) & N_{23} &= \frac{-6\zeta}{l}(\zeta - 1) \\ N_{14} &= l\zeta(-\zeta + \zeta^2) & N_{24} &= -2\zeta + 3\zeta^2 \end{aligned}$$

and still $\zeta = z/l$. Neglecting the shear deformation and from Eq (3.17), the strain can be linked to the displacement as:

$$\epsilon(z) = \frac{\partial^2 u_x}{\partial z^2} = \frac{\partial \theta_y}{\partial z} = 2\alpha_3 + 6\alpha_4 z \quad (3.20)$$

Then

$$\epsilon(z) = [0 \quad 0 \quad 2 \quad 6z] \begin{Bmatrix} \alpha_1 \\ \alpha_2 \\ \alpha_3 \\ \alpha_4 \end{Bmatrix} = [C]\{\alpha\} \quad (3.21)$$

From Eqs (3.19) and (3.21):

$$\epsilon(z) = [C][A]^{-1}\{q_{F1}\} = [B]\{q_{F1}\} \quad (3.22)$$

The relationship between bending stress and strain can be written as:

$$\sigma(z) = \mathbf{E}\epsilon(z) = EI_y \left(\frac{\partial^2 u_x}{\partial z^2} \right)$$

Then, the stiffness of the material \mathbf{E} is

$$\mathbf{E} = EI_y$$

Adopting the Eq (3.5), for each element the stiffness matrix is:

$$K_{XZ} = \int B^T \mathbf{E} B dV = \frac{EI}{l^3} \begin{bmatrix} 12 & 6l & -12 & 6l \\ 6l & 4l^2 & -6l & 2l^2 \\ -12 & -6l & 12 & -6l \\ 6l & 2l^2 & -6l & 4l^2 \end{bmatrix} \quad (3.23)$$

Considering the rotation, the kinetic energy of the beam with the length of dz is then:

$$\begin{aligned} d\mathcal{T} &= \frac{1}{2} \rho A \dot{u}_x^2 dz + \frac{1}{2} \rho I_y \dot{\theta}_y^2 dz = \\ &= \frac{1}{2} \rho A \dot{q}^T N_1^T N_1 \dot{q} dz + \frac{1}{2} \rho I_y \dot{q}^T N_2^T N_2 \dot{q} dz \end{aligned} \quad (3.24)$$

where N_1 , and N_2 represent the first and second rows of matrix N_{F1} respectively.

Following the same logic as in Eq (3.7):

$$\mathcal{T} = \frac{1}{2} \rho A \dot{q}^T \left(\int_0^l N_1^T N_1 dz \right) \dot{q} + \frac{1}{2} \rho I_y \dot{q}^T \left(\int_0^l N_2^T N_2 dz \right) \dot{q} \quad (3.25)$$

Then the mass matrix can be expressed as:

$$M_{xz} = \frac{\rho Al}{420} \begin{bmatrix} m_1 & lm_2 & m_3 & -lm_4 \\ lm_2 & l^2m_5 & lm_4 & -l^2m_6 \\ m_3 & lm_4 & m_1 & -lm_2 \\ -lm_4 & -l^2m_6 & -lm_2 & l^2m_5 \end{bmatrix} + \frac{\rho l y}{30l} \begin{bmatrix} m_7 & lm_8 & -m_7 & lm_8 \\ lm_8 & l^2m_9 & -lm_8 & l^2m_{10} \\ -m_7 & -lm_8 & m_7 & -lm_8 \\ lm_8 & l^2m_{10} & -lm_8 & l^2m_9 \end{bmatrix} \quad (3.26)$$

Where m_i , the coefficients of the mass matrix, are obtained substituting the expression of the shape function into kinetic energy and integrating it.

The mass coefficient expressions are:

$$\begin{aligned} m_1 &= 156 & m_6 &= 3 \\ m_2 &= 22 & m_7 &= 36 \\ m_3 &= 54 & m_8 &= 3 \\ m_4 &= 13 & m_9 &= 4 \\ m_5 &= 4 & m_{10} &= 1 \end{aligned}$$

The load vector due to distributed shear force $f_x(t)$ and bending moment $m_y(t)$ would be:

$$\mathbf{f}(t)_{F1} = \frac{l f_x(t)}{12} \begin{Bmatrix} 6 \\ l \\ 6 \\ -l \end{Bmatrix} + m_y(t) \begin{Bmatrix} -l \\ 0 \\ l \\ 0 \end{Bmatrix}$$

Flexural behavior – yz plane

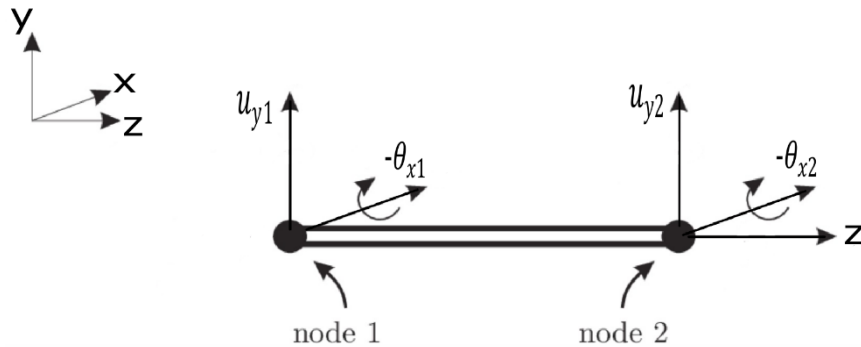


Figure 3-5 _ Euler-Bernoulli beam element and flexural degrees of freedom within yz plane

In this case, as what has been discussed about flexural behavior in the xz-plane, to each node are associated two DOFs a translational one along the y axis (u_y) and a rotational one around the x axis (θ_x). This means that the mass, stiffness, and damping matrices associated with this discretized element have a 4×4 size. Due to different signs of rotations, we need to use equations different from those in the xz-plane.

The matrices, in this case, could easily be obtained from those achieved for xz-plane by a simple change of signs of elements with subscripts 12, 14, 21, and 23 in shape function matrix N_{F1} and either the elements with subscripts 12, 14, 23, and 34 and their symmetrical ones in mass and stiffness matrices. With respect to external force vector, and external moments, we only need to change the signs of elements 2 and 4 or 1 and 3.

$$\{q_{F2}\} = \{u_{y1} \ \theta_{x1} \ u_{y2} \ \theta_{x2}\}'_{1 \times 4} \quad N_{F2} = \begin{bmatrix} N_{11} & -N_{12} & N_{13} & -N_{14} \\ -N_{21} & N_{22} & -N_{23} & N_{24} \end{bmatrix}$$

For each element the stiffness matrix is:

$$\mathbf{K}_{yz} = \frac{EI}{l^3} \begin{bmatrix} 12 & -6l & -12 & -6l \\ -6l & 4l^2 & 6l & 2l^2 \\ -12 & 6l & 12 & 6l \\ -6l & 2l^2 & 6l & 4l^2 \end{bmatrix} \quad (3.27)$$

While the mass matrix, since we adopted a consistent mass matrix approach, is given by:

$$\mathbf{M}_{yz} = \frac{\rho Al}{420} \begin{bmatrix} m_1 & -lm_2 & m_3 & lm_4 \\ -lm_2 & l^2m_5 & -lm_4 & -l^2m_6 \\ m_3 & -lm_4 & m_1 & lm_2 \\ lm_4 & -l^2m_6 & lm_2 & l^2m_5 \end{bmatrix} + \frac{\rho I_x}{30l} \begin{bmatrix} m_7 & -lm_8 & -m_7 & -lm_8 \\ -lm_8 & l^2m_9 & lm_8 & l^2m_{10} \\ -m_7 & lm_8 & m_7 & lm_8 \\ -lm_8 & l^2m_{10} & lm_8 & l^2m_9 \end{bmatrix} \quad (3.28)$$

The load vector due to distributed shear force $f_y(t)$ and bending moment $m_x(t)$ would be:

$$\mathbf{f}(t)_{F2} = \frac{lf_y(t)}{12} \begin{Bmatrix} 6 \\ -l \\ 6 \\ l \end{Bmatrix} + m_x(t) \begin{Bmatrix} -l \\ 0 \\ l \\ 0 \end{Bmatrix}$$

3.1.2 Effect of axial force on flexural behavior

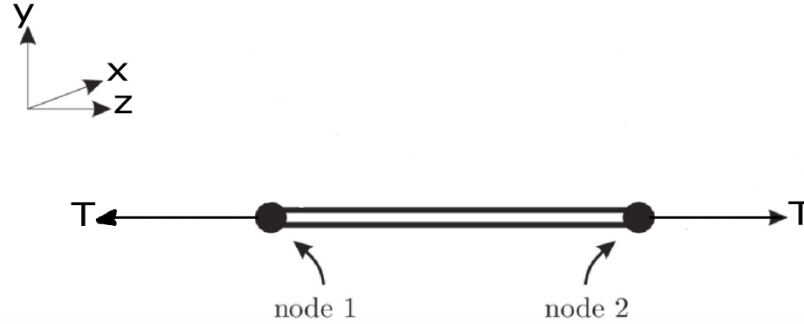


Figure 3-6 _ Euler-Bernoulli beam element with axial force T

The interaction between flexural behavior and axial force in a beam causes geometric nonlinearity. To avoid this nonlinearity, in the case of constant axial load, it is possible to linearize the interaction.

Considering the flexural behavior of the Euler-Bernoulli beam on xz-plane, and a constant and known axial tensile load T applied on it, the axial strain with respect to the neutral axis of the beam becomes:

$$\epsilon_z = \frac{\partial u_z}{\partial z} + \frac{1}{2} \left(\frac{\partial u_y}{\partial z} \right)^2 \quad (3.28)$$

Writing the elastic potential energy due the strain:

$$U = \frac{1}{2} \int_0^l EA \epsilon_z^2 dz = \frac{1}{2} \int_0^l EA \left[\frac{\partial u_z}{\partial z} + \frac{1}{2} \left(\frac{\partial u_y}{\partial z} \right)^2 \right]^2 dz \approx \frac{1}{2} \int_0^l EA \left(\frac{\partial u_z}{\partial z} \right)^2 dz + \frac{1}{2} \int_0^l EA \frac{\partial u_z}{\partial z} \left(\frac{\partial u_y}{\partial z} \right)^2 dz \quad (3.28)$$

In the last expression the term $\left(\frac{\partial u_y}{\partial z} \right)^4$ was neglected.

In Eq (3.28), the first term has already been included in the computation of the stiffness matrix of the element and the second term is the increment of the potential energy, which can be taken into account by adding a so-called geometric stiffness matrix to the stiffness matrix of the element.

Since the axial force $T = \epsilon_z EA$, is constant, using the shape functions, this incremented stiffness can be calculated through the following procedure:

$$\Delta U = \frac{1}{2} \epsilon_z \int_0^l EA \left(\frac{\partial u_y}{\partial z} \right)^2 dz = \frac{1}{2} T q_{F1}^T K_g q_{F1}$$

where

$$K_g = \frac{T}{30l} \begin{bmatrix} k_1 & lk_2 & -k_1 & lk_2 \\ lk_2 & l^2k_3 & -lk_2 & -l^2k_4 \\ -k_1 & -lk_2 & k_1 & -lk_2 \\ lk_2 & -l^2k_4 & -lk_2 & l^2k_3 \end{bmatrix} \quad (3.29)$$

$$k_1 = 36$$

$$k_2 = 3$$

$$k_3 = 4$$

$$k_4 = 1$$

Simply by adding this matrix to the bending stiffness of the element either in xz or yz planes, we discussed earlier, the total stiffness of the matrix will be achieved.

3.2 Time Integration: Newmark Scheme for dynamic study

Newmark is a second order basic scheme to discretize a second order time system and perform integration in discrete time. It is applied to the following problem:

$$\begin{cases} \mathbf{M}\ddot{\mathbf{q}} + \mathbf{C}\dot{\mathbf{q}} + \mathbf{K}\mathbf{q} = \mathbf{f}(t) \\ \mathbf{q}_0, \dot{\mathbf{q}}_0 \quad \text{given} \end{cases} \quad (3.30)$$

According to (M. Géradin, D. Rixen , 1997), we have the approximation formulas as:

$$\boxed{\begin{aligned} \dot{\mathbf{q}}_{n+1} &= \dot{\mathbf{q}}_n + (1 - \gamma)h\ddot{\mathbf{q}}_n + \gamma h\ddot{\mathbf{q}}_{n+1} \\ \mathbf{q}_{n+1} &= \mathbf{q}_n + h\dot{\mathbf{q}}_n + h^2\left(\frac{1}{2} - \beta\right)\ddot{\mathbf{q}}_n + h^2\beta\ddot{\mathbf{q}}_{n+1} \end{aligned}} \quad (3.31)$$

While $h = t_{n+1} - t_n$ is time step size, and β and γ are parameters adopted to ensure the stability, assuming the following values:

$$\beta = \frac{1}{4} \quad \gamma = \frac{1}{2}$$

In case the dynamic equations (3.1) are linear, by introducing the scheme (3.2) in the equation of motion at time t_{n+1} we will have:

$$\begin{aligned} [\mathbf{M} + \gamma h\mathbf{C} + \beta h^2\mathbf{K}]\ddot{\mathbf{q}}_{n+1} &= \mathbf{f}_{n+1} - \mathbf{C}[\dot{\mathbf{q}}_n + (1 - \gamma)h\ddot{\mathbf{q}}_n] \\ &\quad - \mathbf{K}\left[\mathbf{q}_n + h\dot{\mathbf{q}}_n + \left(\frac{1}{2} - \beta\right)h^2\ddot{\mathbf{q}}_n\right] \end{aligned} \quad (3.32)$$

The matrix $[\mathbf{M} + \gamma h\mathbf{C} + \beta h^2\mathbf{K}]$ is the iteration matrix which, due to properties of matrices \mathbf{M} , \mathbf{K} , and \mathbf{C} , is positive definite and symmetric.

A summary of the Newmark scheme for time integration of equation (3.30) is represented here in form of a flowchart. In prior, in the sake of more efficiency, we introduce the predictors \dot{q}_{n+1}^* and q_{n+1}^* as:

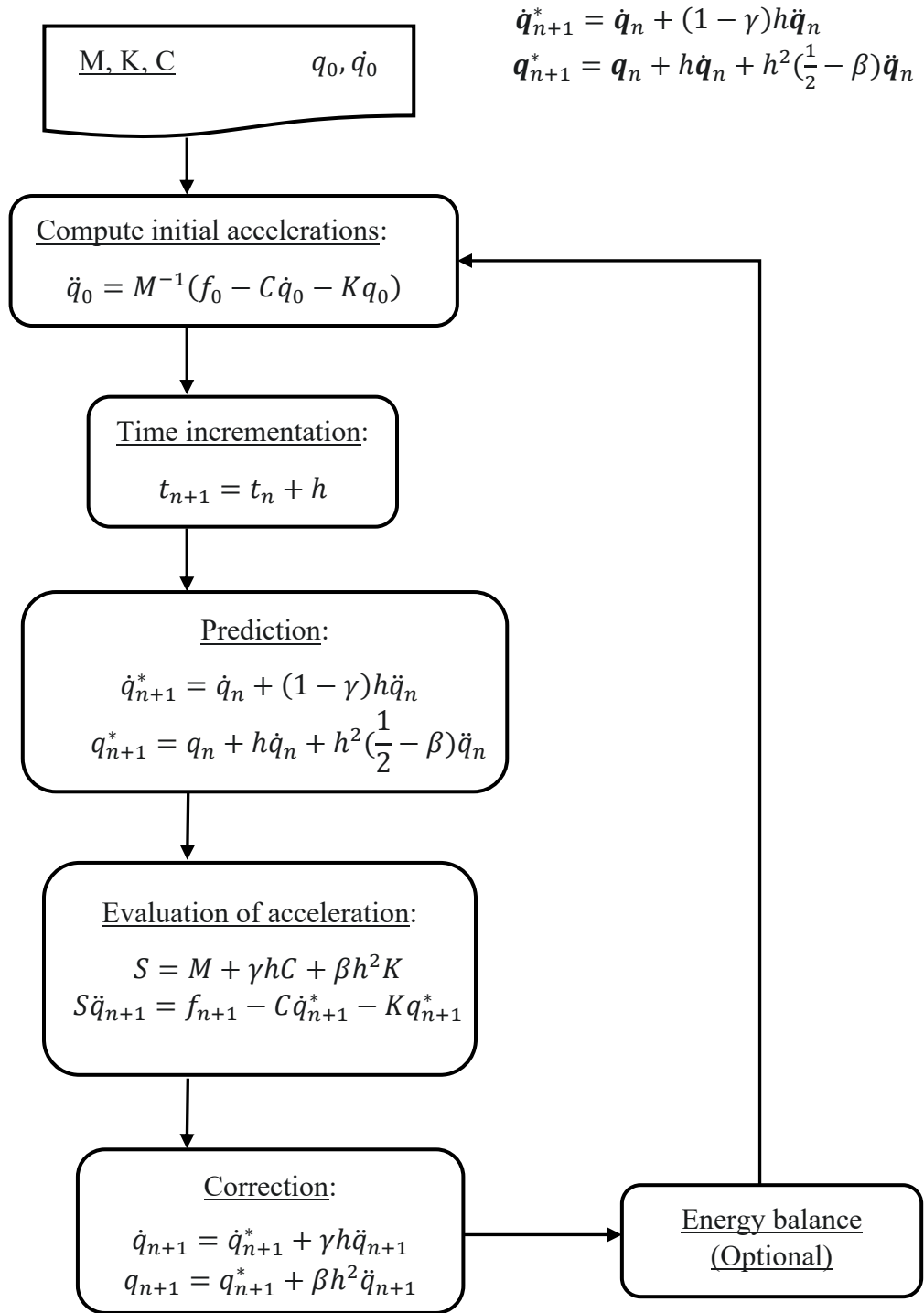


Figure 3-7 _ Flowchart – Newmark integration for linear systems

4 1st Configuration: Single-Span cable

The reference system that is going to be simulated and studied in this chapter is a single-span cable taut with a tensile load T (pretension) which is clamped at the left-end side. All the degrees of freedoms on the right-end side, are locked except for the axial displacement to prevent singularity in matrices. The study consists of modal analysis, step response, harmonic response, and response to moving load. In the following the table 4.1 reports the geometrical data and some other properties of the systems.

Table 4.1 _ Geometrical data and parameters of the system

Density	$\rho = 8940 \frac{kg}{m^3}$	mass per unit of length	$\mu = \rho \times \pi R^2 = 7.19 \frac{kg}{m}$
Elastic modulus	$E = 120 \times 10^9 \text{ Pa}$	Span length	$l = 6 \text{ m}$
Diameter	$D = 32 \times 10^{-3} \text{ m}$	Pretension	$T = 100 \text{ kN}$

4.1 Implementation of Euler-Bernoulli beam element

4.1.1 Global behavior of the beam

In this case, a beam with general orientation in space has been considered. A global reference of frame O (XYZ) is defined so that the gravity field is directed toward the negative sign of the X -axis. In figure 4.1, a general beam with its local reference frame O' and global reference frame O is depicted.

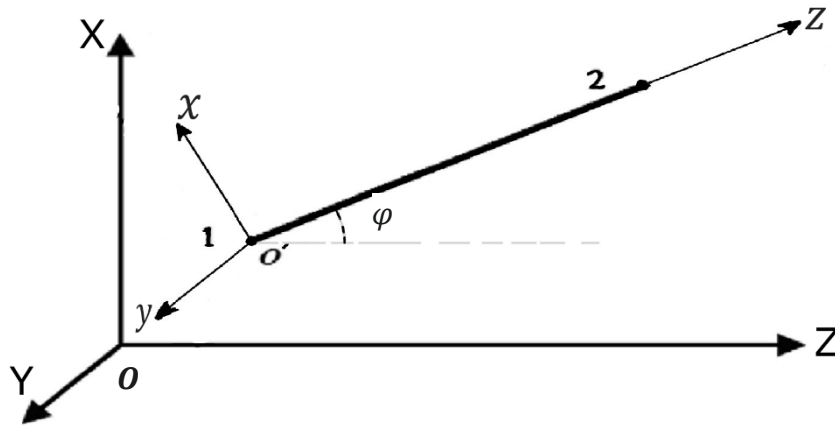


Figure 4-1 _ General E-B beam element with local and global reference frame respectively O and O'

The global reference frame O (XYZ) and the local reference frame O' (xyz) have been defined so that the beam locates on the XZ plane of the frame O , and the y -axis of frame O' has the same direction as Y -axis in O frame. In this way, the beam has an inclination of angle φ with respect to axis Y . This logic will help us to drive the equation of motion of the beam with respect to the global reference frame.

The total expression of the mass and stiffness matrices associated with the adopted discretized element have a 12×12 size and will be as following:

$$\begin{bmatrix} ma_{1,1} & 0 & 0 & 0 & 0 & 0 & ma_{1,2} & 0 & 0 & 0 & 0 & 0 \\ 0 & mfx_{1,1} & 0 & 0 & 0 & mfx_{1,2} & 0 & mfx_{1,3} & 0 & 0 & 0 & mfx_{1,4} \\ 0 & 0 & mfy_{1,1} & 0 & mfy_{1,2} & 0 & 0 & 0 & mfy_{1,3} & 0 & mfy_{1,4} & 0 \\ 0 & 0 & 0 & mt_{1,1} & 0 & 0 & 0 & 0 & 0 & mt_{1,2} & 0 & 0 \\ 0 & 0 & mfy_{2,1} & 0 & mfy_{2,2} & 0 & 0 & 0 & mfy_{2,3} & 0 & mfy_{2,4} & 0 \\ 0 & mfx_{2,1} & 0 & 0 & 0 & mfx_{2,2} & 0 & mfx_{2,3} & 0 & 0 & 0 & mfx_{2,4} \\ ma_{2,1} & 0 & 0 & 0 & 0 & 0 & ma_{2,2} & 0 & 0 & 0 & 0 & 0 \\ 0 & mfx_{3,1} & 0 & 0 & 0 & mfx_{3,2} & 0 & mfx_{3,3} & 0 & 0 & 0 & mfx_{3,4} \\ 0 & 0 & mfy_{3,1} & 0 & mfy_{3,2} & 0 & 0 & 0 & mfy_{3,3} & 0 & mfy_{3,4} & 0 \\ 0 & 0 & 0 & mt_{2,1} & 0 & 0 & 0 & 0 & 0 & mt_{2,2} & 0 & 0 \\ 0 & 0 & mfy_{4,1} & 0 & mfy_{4,2} & 0 & 0 & 0 & mfy_{4,3} & 0 & mfy_{4,4} & 0 \\ 0 & mfx_{4,1} & 0 & 0 & 0 & mfx_{4,2} & 0 & mfx_{4,3} & 0 & 0 & 0 & mfx_{4,4} \end{bmatrix} \begin{Bmatrix} u_{z1} \\ u_{x1} \\ u_{y1} \\ \theta_{z1} \\ \theta_{x1} \\ \theta_{y1} \\ u_{z2} \\ u_{x2} \\ u_{y2} \\ \theta_{z2} \\ \theta_{x2} \\ \theta_{y2} \end{Bmatrix}$$

$$\{q\} = \{u_{z1} \ u_{x1} \ u_{y1} \ \theta_{z1} \ \theta_{x1} \ \theta_{y1} \ u_{z2} \ u_{x2} \ u_{y2} \ \theta_{z2} \ \theta_{x2} \ \theta_{y2}\}'_{1 \times 12}$$

In which $ma_{n,m}$ stands for elements in the M_A , $mt_{n,m}$ stands for elements in M_T , $mfx_{n,m}$ for elements in the M_{xz} , and $mfy_{n,m}$ for elements in M_{yz} .

Here is the complete mass matrix of the element is expressed and the same configuration holds for the total stiffness matrix of the element.

$$\begin{bmatrix} ka_{1,1} & 0 & 0 & 0 & 0 & 0 & ka_{1,2} & 0 & 0 & 0 & 0 & 0 \\ 0 & kfx_{1,1} & 0 & 0 & 0 & kfx_{1,2} & 0 & kfx_{1,3} & 0 & 0 & 0 & kfx_{1,4} \\ 0 & 0 & kfy_{1,1} & 0 & kfy_{1,2} & 0 & 0 & 0 & kfy_{1,3} & 0 & kfy_{1,4} & 0 \\ 0 & 0 & 0 & kt_{1,1} & 0 & 0 & 0 & 0 & 0 & kt_{1,2} & 0 & 0 \\ 0 & 0 & kfy_{2,1} & 0 & kfy_{2,2} & 0 & 0 & 0 & kfy_{2,3} & 0 & kfy_{2,4} & 0 \\ 0 & kfx_{2,1} & 0 & 0 & 0 & kfx_{2,2} & 0 & kfx_{2,3} & 0 & 0 & 0 & kfx_{2,4} \\ ka_{2,1} & 0 & 0 & 0 & 0 & 0 & ka_{2,2} & 0 & 0 & 0 & 0 & 0 \\ 0 & kfx_{3,1} & 0 & 0 & 0 & kfx_{3,2} & 0 & kfx_{3,3} & 0 & 0 & 0 & kfx_{3,4} \\ 0 & 0 & kfy_{3,1} & 0 & kfy_{3,2} & 0 & 0 & 0 & kfy_{3,3} & 0 & kfy_{3,4} & 0 \\ 0 & 0 & 0 & kt_{2,1} & 0 & 0 & 0 & 0 & 0 & kt_{2,2} & 0 & 0 \\ 0 & 0 & kfy_{4,1} & 0 & kfy_{4,2} & 0 & 0 & 0 & kfy_{4,3} & 0 & kfy_{4,4} & 0 \\ 0 & kfx_{4,1} & 0 & 0 & 0 & kfx_{4,2} & 0 & kfx_{4,3} & 0 & 0 & 0 & kfx_{4,4} \end{bmatrix} \begin{Bmatrix} u_{z1} \\ u_{x1} \\ u_{y1} \\ \theta_{z1} \\ \theta_{x1} \\ \theta_{y1} \\ u_{z2} \\ u_{x2} \\ u_{y2} \\ \theta_{z2} \\ \theta_{x2} \\ \theta_{y2} \end{Bmatrix}$$

In which $ka_{n,m}$ stands for elements in the K_A , $kt_{n,m}$ stands for elements in K_T , $kfx_{n,m}$ for elements in the K_{xz} , and $kfy_{n,m}$ for elements in K_{yz} .

The complete expression for the nodal force vector for an inclined single beam element with respect to its local reference frame under pretension T is:

$$\mathbf{f} = \left\{ \left(-T - \frac{pl}{2} \sin \varphi \right) \quad \frac{pl}{2} \cos \varphi \quad 0 \quad 0 \quad 0 \quad \frac{pl^2}{12} \cos \varphi \quad \left(T - \frac{pl}{2} \sin \varphi \right) \quad \frac{pl}{2} \cos \varphi \quad 0 \quad 0 \quad 0 \quad -\frac{pl^2}{12} \cos \varphi \right\}_{1 \times 12}$$

Where T is the tensile load, $p = \mu g$ is the weight per unit length of the beam, and l is the length of the element.

As a result, the equation of motion of the element with respect to its local reference frame is as:

$$\mathbf{M}_l \ddot{\mathbf{q}}_l + \mathbf{K}_l \mathbf{q}_l = \mathbf{f}_l(t) \quad (4.1)$$

And \mathbf{M}_l , and \mathbf{K}_l are the mass, and stiffness matrices of the element with respect to the local reference frame.

4.1.2 From local to global reference frame and rotation matrices

The orientation of the local reference frame with respect to the global one is expressed by an appropriate rotation matrix. The vectors q_{i_g} and q_{i_l} , which are respectively the coordinate vectors of the i th node with respect to the global and local reference frames, can be linked through appropriate transformation.

According to figure 4.1, the rotation matrix representing the orientation of the local reference frame with respect to the global one is:

$$\mathbf{R} = \begin{bmatrix} \cos \varphi & \sin \varphi & 0 \\ -\sin \varphi & \cos \varphi & 0 \\ 0 & 0 & 1 \end{bmatrix}$$

The transformation can be expressed as:

$$\mathbf{q}_{i_l} = \mathbf{R}\mathbf{q}_{i_g} \quad (4.2)$$

In order to transfer the displacement vector of the element which has a dimension of 12×1 , the expanded rotation matrix \mathbf{R}' with a similar transformation is used. The expanded rotation matrix \mathbf{R}' has a structure as the following:

$$\mathbf{R}' = \begin{bmatrix} [\mathbf{R}_{3 \times 3}] & [\mathbf{0}_{3 \times 3}] & [\mathbf{0}_{3 \times 3}] & [\mathbf{0}_{3 \times 3}] \\ [\mathbf{0}_{3 \times 3}] & [\mathbf{R}_{3 \times 3}] & [\mathbf{0}_{3 \times 3}] & [\mathbf{0}_{3 \times 3}] \\ [\mathbf{0}_{3 \times 3}] & [\mathbf{0}_{3 \times 3}] & [\mathbf{R}_{3 \times 3}] & [\mathbf{0}_{3 \times 3}] \\ [\mathbf{0}_{3 \times 3}] & [\mathbf{0}_{3 \times 3}] & [\mathbf{0}_{3 \times 3}] & [\mathbf{R}_{3 \times 3}] \end{bmatrix}_{12 \times 12}$$

To write the equation of the motion with respect to the global reference frame, we start from equation 4.1 which describes the behavior of the structure in the local reference frame. By implementing the transformation equation 4.2, we get:

$$\mathbf{R}'^{-1}\mathbf{M}\mathbf{R}'\ddot{\mathbf{q}}_g + \mathbf{R}'^{-1}\mathbf{K}\mathbf{R}'\mathbf{q}_g = \mathbf{f}_g \quad (4.3)$$

As the inverse of a rotation matrix is identical to its transpose, the global force vector, as well as the global mass and stiffness matrices can be expressed as:

$$\begin{aligned} \mathbf{M}_g &= \mathbf{R}'^T \mathbf{M}_l \mathbf{R}' \\ \mathbf{K}_g &= \mathbf{R}'^T \mathbf{K}_l \mathbf{R}' \\ \mathbf{f}_g &= \mathbf{R}'^T \mathbf{f}_l \end{aligned} \quad (4.4)$$

4.1.3 Assembling and mapping matrices

After defining the elements mass and stiffness matrices in the local reference frame of the element, the global matrices must be assembled. The beam shown in the figure 4.1 has two symmetry planes in XZ and YZ plane and motion is supposed to be decoupled in XZ plane, YZ plane, axial displacement, and rotation along Z-axis.

To illustrate more clearly, the beam can be discretized into three elements (1,2,3) and four nodes (1,2,3,4). The correct number of elements in the MATLAB code is much higher so that the global matrices' dimension will be of thousands.

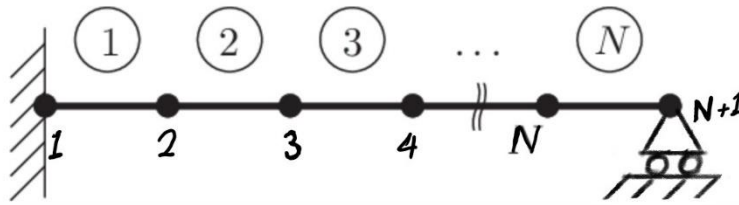


Figure 4-2 _single-span cable modelled as a beam of N E-B elements

As it was discussed already, to each node are associated six DoFs. This means that the mass, stiffness and damping matrices associated to each discretized element have a 12×12 size while the global matrix of whole structure has a 24×24 size. The DoF arrangement will be:

$$\{q\} = \{u_{z1} \ u_{x1} \ u_{y1} \ \theta_{z1} \ \theta_{x1} \ \theta_{y1} \ \dots \ u_{z4} \ u_{x4} \ u_{y4} \ \theta_{z4} \ \theta_{x4} \ \theta_{y4}\}'_{1 \times 24}$$

In general, a so-called Map Matrix helps to move from individual elements to the whole structure. In our example with only three elements the map matrix would be the following:

The global mass and stiffness matrices of the whole structure \mathbf{M}_T and \mathbf{K}_T and the global nodal force vector \mathbf{f}_T are achieved by this assembling approach. In the picture below, the final structure of the total stiffness matrix of the structure is depicted which is identical to that of the total mass matrix.

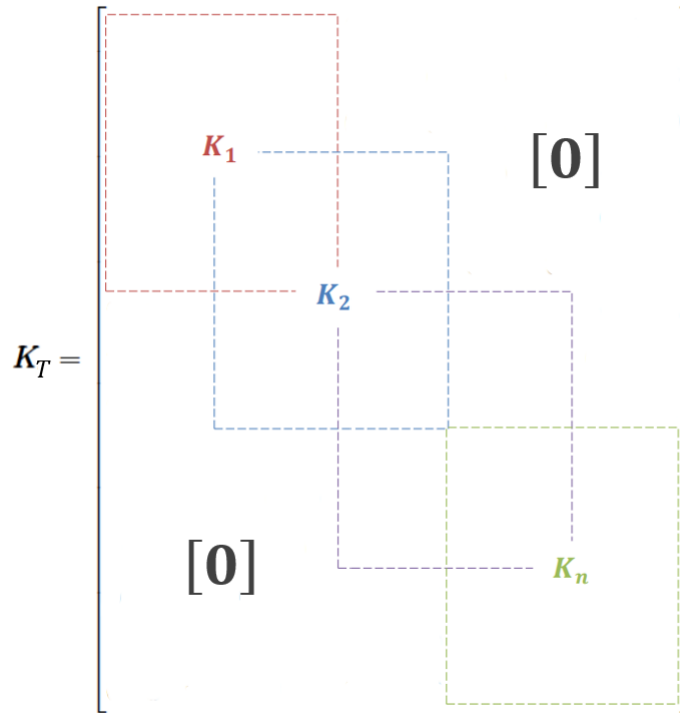


Figure 4-3 _ Total stiffness matrix of the structure configuration

As a result, the global equation of motion of the entire structure is:

$$\mathbf{M}_T \ddot{\mathbf{q}} + \mathbf{K}_T \mathbf{q} = \mathbf{f}(t) \quad (4.5)$$

From this moment on, vector \mathbf{q} represents the global nodal displacement vector of the whole structure.

Now that we have written the equation of motion and mass and stiffness matrices of the whole structure with respect to the global reference frame, the possibility of introducing damping effect can be considered adopting the proportional damping matrix \mathbf{C}_T as following:

$$\mathbf{C}_T = \alpha \mathbf{M}_T + \beta \mathbf{K}_T \quad (4.6)$$

Then the equation of motion will become:

$$\mathbf{M}_T \ddot{\mathbf{q}} + \mathbf{C}_T \dot{\mathbf{q}} + \mathbf{K}_T \mathbf{q} = \mathbf{f}(t) \quad (4.7)$$

4.2 Boundary Conditions and Static equilibrium

Due to the presence of the clamped constraint at the starting node and blocking all the degrees of freedom except for the axial displacement at the ending node for the sake of preventing singular matrices, as a result, almost null displacement and rotation occur at those DoF's. In our example:

$$\{q_1\} = \begin{Bmatrix} u_{z1} \\ u_{x1} \\ u_{y1} \\ \theta_{z1} \\ \theta_{x1} \\ \theta_{y1} \end{Bmatrix} = \begin{Bmatrix} 0 \\ 0 \\ 0 \\ 0 \\ 0 \\ 0 \end{Bmatrix} \quad \{q_4\} = \begin{Bmatrix} u_{z1} \\ u_{x1} \\ u_{y1} \\ \theta_{z1} \\ \theta_{x1} \\ \theta_{y1} \end{Bmatrix} = \begin{Bmatrix} u_{z1} \\ 0 \\ 0 \\ 0 \\ 0 \\ 0 \end{Bmatrix}$$

There are two approaches to implement the constraints. The first solution is to reduce the dimension of both global mass and global stiffness matrices of the structure by cancelling the corresponding rows and columns of the constrained degrees of freedom. Advantage of this approach is a quick and easy numerical simulation but, it could not represent the reality of the constraints.

The second solution enables the simulation to be closer to the reality. In this approach, instead of cancelling any DoFs, we introduce strong relevant stiffness at that DoF. The selected value for this additional stiffness must represent infinity compared to other related stiffness values. This method still has its own disadvantages.

By adding high values of stiffnesses, practically we introduce very high values of frequencies to the system, under the numerical point of view, so that time step must be settled extremely small, and this makes very expensive simulation in the matter of time.

Adopting the second solution, k and χ are symbols adopted for added stiffnesses implemented respectively on translational and rotational DoFs. For instance, χ_{z1} is the added translational stiffness to the torsion about z direction (the axis of the beam) at the first node. As a result, all the additional stiffnesses are as the following:

$$\{k_{z1} \ k_{x1} \ k_{y1} \ \chi_{z1} \ \chi_{x1} \ \chi_{y1} \ k_{x4} \ k_{y4} \ \chi_{z4} \ \chi_{x4} \ \chi_{y4}\}$$

Incrementation of potential energy due to additional stiffnesses is:

$$\begin{aligned} \Delta U = & \frac{1}{2}k_{z1}(u_{z1})^2 + \frac{1}{2}k_{x1}(u_{x1})^2 + \frac{1}{2}k_{y1}(u_{y1})^2 + \frac{1}{2}\chi_{z1}(\theta_{z1})^2 + \frac{1}{2}\chi_{x1}(\theta_{x1})^2 + \frac{1}{2}\chi_{y1}(\theta_{y1})^2 + \dots \\ & \dots + \frac{1}{2}k_{x4}(u_{x4})^2 + \frac{1}{2}k_{y4}(u_{y4})^2 + \frac{1}{2}\chi_{z4}(\theta_{z4})^2 + \frac{1}{2}\chi_{x4}(\theta_{x4})^2 + \frac{1}{2}\chi_{y4}(\theta_{y4})^2 \end{aligned}$$

The stiffnesses representing the boundary conditions will modify global stiffness matrix:

$$\begin{array}{ll} \frac{d}{dt} \left(\frac{\partial \Delta U}{\partial u_{z1}} \right) = k_{z1} u_{z1} & \frac{d}{dt} \left(\frac{\partial \Delta U}{\partial u_{z4}} \right) = k_{z4} u_{z4} \\ \frac{d}{dt} \left(\frac{\partial \Delta U}{\partial u_{x1}} \right) = k_{x1} u_{x1} & \frac{d}{dt} \left(\frac{\partial \Delta U}{\partial u_{y4}} \right) = k_{y4} u_{y4} \\ \frac{d}{dt} \left(\frac{\partial \Delta U}{\partial u_{y1}} \right) = k_{y1} u_{y1} & \frac{d}{dt} \left(\frac{\partial \Delta U}{\partial \theta_{z4}} \right) = \chi_{z4} \theta_{z4} \\ \frac{d}{dt} \left(\frac{\partial \Delta U}{\partial \theta_{z1}} \right) = \chi_{z1} \theta_{z1} & \frac{d}{dt} \left(\frac{\partial \Delta U}{\partial \theta_{x4}} \right) = \chi_{x4} \theta_{x4} \\ \frac{d}{dt} \left(\frac{\partial \Delta U}{\partial \theta_{x1}} \right) = \chi_{x1} \theta_{x1} & \frac{d}{dt} \left(\frac{\partial \Delta U}{\partial \theta_{y4}} \right) = \chi_{y4} \theta_{y4} \\ \frac{d}{dt} \left(\frac{\partial \Delta U}{\partial \theta_{y1}} \right) = \chi_{y1} \theta_{y1} & \end{array}$$

Since in our case the added stiffnesses does not link the corresponding DoFs to another DoFs, these values are added to the relative array on the main diagonal of stiffness matrix:

$$\begin{bmatrix}
 \blacksquare + k_{z1} & \blacksquare & \blacksquare & \blacksquare & \blacksquare & \blacksquare & \cdots & 0 & 0 \\
 \blacksquare & \blacksquare + k_{x1} & \blacksquare & \blacksquare & \blacksquare & \blacksquare & \cdots & 0 & 0 \\
 \blacksquare & \blacksquare & \blacksquare + k_{y1} & \blacksquare & \blacksquare & \blacksquare & \cdots & 0 & 0 \\
 \blacksquare & \blacksquare & \blacksquare & \blacksquare + \chi_{z1} & \blacksquare & \blacksquare & \cdots & 0 & 0 \\
 \blacksquare & \blacksquare & \blacksquare & \blacksquare & \blacksquare + \chi_{x1} & \blacksquare & \cdots & 0 & 0 \\
 \blacksquare & \blacksquare & \blacksquare & \blacksquare & \blacksquare & \blacksquare + \chi_{y1} & \cdots & 0 & 0 \\
 \vdots & \vdots & \vdots & \vdots & \vdots & \vdots & \ddots & \vdots & \vdots \\
 0 & 0 & 0 & 0 & 0 & 0 & \cdots & \blacksquare + \chi_{x4} & \blacksquare \\
 0 & 0 & 0 & 0 & 0 & 0 & \cdots & \blacksquare & \blacksquare + \chi_{y4}
 \end{bmatrix}
 \begin{Bmatrix}
 u_{z1} \\
 u_{x1} \\
 u_{y1} \\
 \theta_{z1} \\
 \theta_{x1} \\
 \theta_{y1} \\
 \vdots \\
 \theta_{x24} \\
 \theta_{y24}
 \end{Bmatrix}$$

4.2.1 Calculation of Static equilibrium and Reaction Forces

The static displacement of the system due to weight of the cable can easily be calculated by solving:

$$\mathbf{K}_T \mathbf{q}_S = \mathbf{f}_T \quad \rightarrow \quad \mathbf{q}_S = \mathbf{K}_T^{-1} \mathbf{f}_T \quad (4.8)$$

where \mathbf{f}_T is the global nodal force vector, \mathbf{K}_T is the global stiffness matrix for the whole structure, and \mathbf{q}_S is the static nodal displacement vector for all the node through the structure.

The displacement calculated using this approach, matches perfectly the results achieved in the thesis (Strauss, 2014) based on continuous method. Figure 4.4 below represents the static equilibrium obtained in this way.

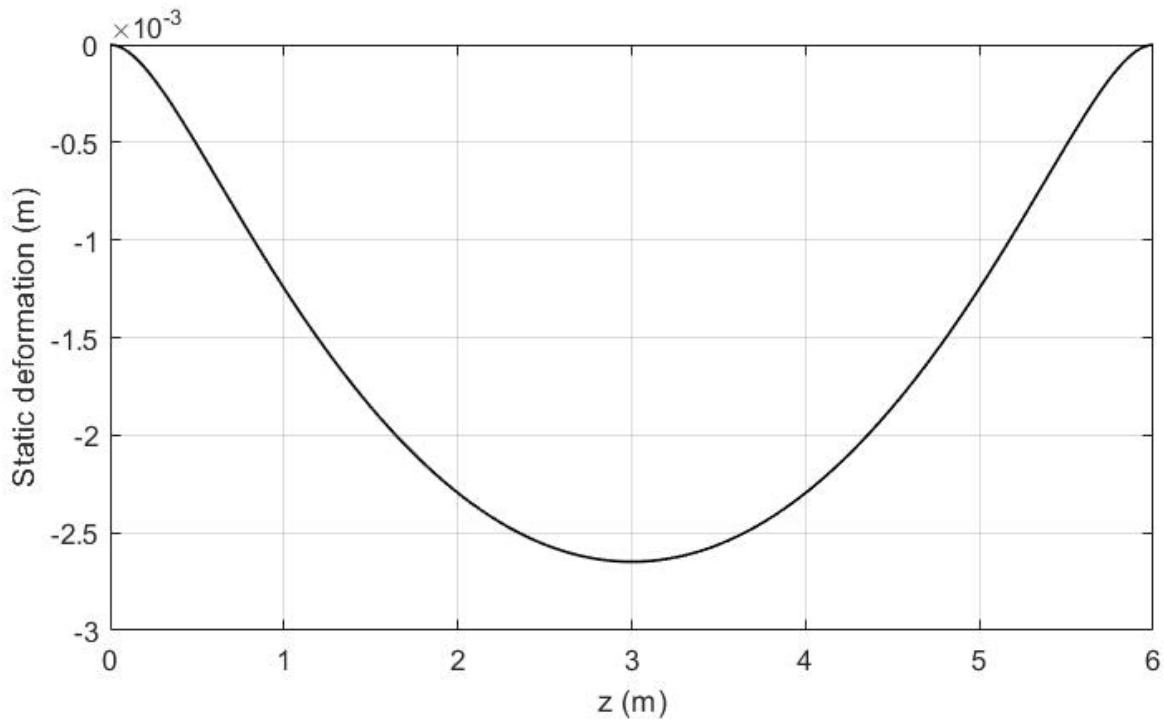


Figure 4-4 _ Static deformation

Reaction forces at the boundaries:

To calculate reaction forces at boundaries, there are two approaches that rely on the method which has been implemented to introduce the boundary conditions:

As the first approach, if the constraints have been introduced by canceling the corresponding rows and columns, the reaction forces can be achieved simply by following these steps:

By cancelling only the columns and not the rows of the stiffness matrix corresponding to those DOFs that have been constrained and eliminating the displacement of those DOFs from the displacement vector, since they are equal to zero, and finally by multiplying the remaining sub-matrix of the stiffness matrix to the remaining sub-vector of the displacement vector, the result can be obtained.

As the constrained DOFs have been introduced by adding strong relevant stiffness values to the corresponding elements of the stiffness matrix, The second approach is implemented as follow:

Since in this case, although the concerned DOFs are constrained but still have small displacements, so by multiplying these small displacements to their corresponding stiffness values, the reaction forces can be calculated. This method is adopted in this work.

With respect to our example described so far:

$$F_{z1} = k_{z1}u_{z1}$$

$$F_{x1} = k_{x1}u_{x1}$$

$$F_{y1} = k_{y1}u_{y1}$$

$$M_{z1} = \chi_{z1}\theta_{z1}$$

$$M_{x1} = \chi_{x1}\theta_{x1}$$

$$M_{y1} = \chi_{y1}\theta_{y1}$$

$$F_{x2} = k_{x2}u_{x2}$$

$$F_{y2} = k_{y2}u_{y2}$$

$$M_{z2} = \chi_{z2}\theta_{z2}$$

$$M_{x2} = \chi_{x2}\theta_{x2}$$

$$M_{y2} = \chi_{y2}\theta_{y2}$$

4.3 Modal analysis of the system and validation

The equation of free motion for an undamped system is:

$$\mathbf{M}_T \ddot{\mathbf{q}}(t) + \mathbf{K}_T \mathbf{q}(t) = \mathbf{0} \quad (4.9)$$

And the solution is in the form of:

$$\mathbf{q}(t) = \boldsymbol{\phi} e^{\omega t}$$

ω_i , and $\boldsymbol{\phi}_i$ are respectively the eigenvalues and eigenvectors. By substituting the solution to the differential equation:

$$(-\omega_i^2 \mathbf{M}_T + \mathbf{K}_T) \boldsymbol{\phi}_i = \mathbf{0} \quad (4.10)$$

Eq (4.10) is the standard eigenvalue problem and calculation of the determinant lead to obtaining the eigenvalues:

$$\det(-\omega^2 \mathbf{M}_T + \mathbf{K}_T) = 0 \quad (4.11)$$

For each ω_i obtained from Eq (4.11), solving Eq (4.10) gives the corresponding eigen vectors $\boldsymbol{\phi}_i$ that are known as i th mode shapes of the system.

In the following, the figures depict the first five modes of the system in the vertical direction.

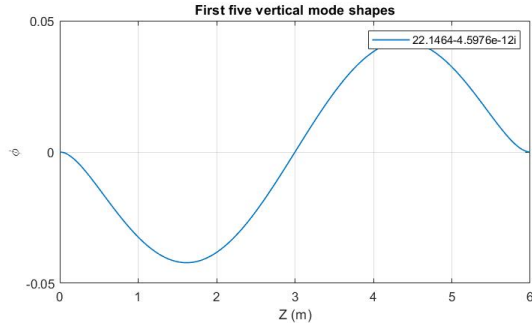


Figure 4-6 _ 2nd vertical mode shape

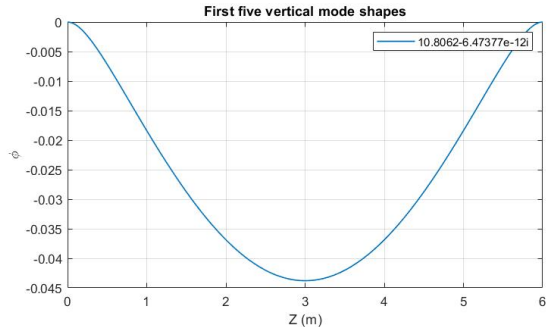


Figure 4-5 _ 1st vertical mode shape

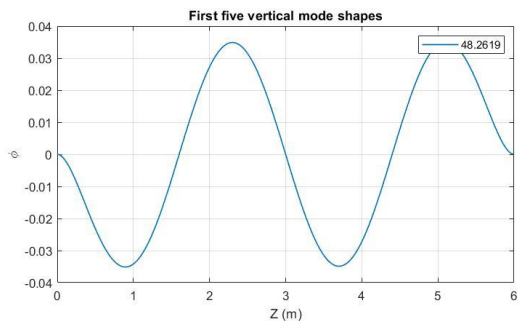


Figure 4-8 _ 4th vertical mode shape

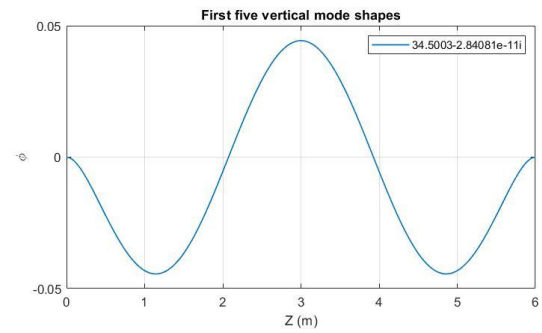


Figure 4-7 _ 3rd vertical mode shape

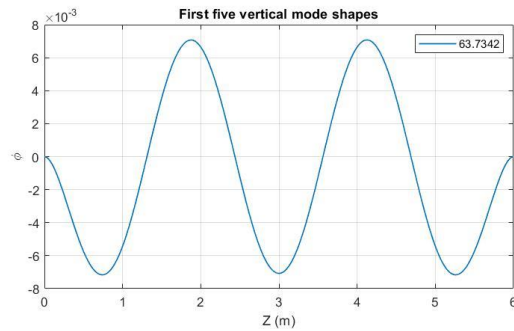


Figure 4-9 _ 5th vertical mode shape

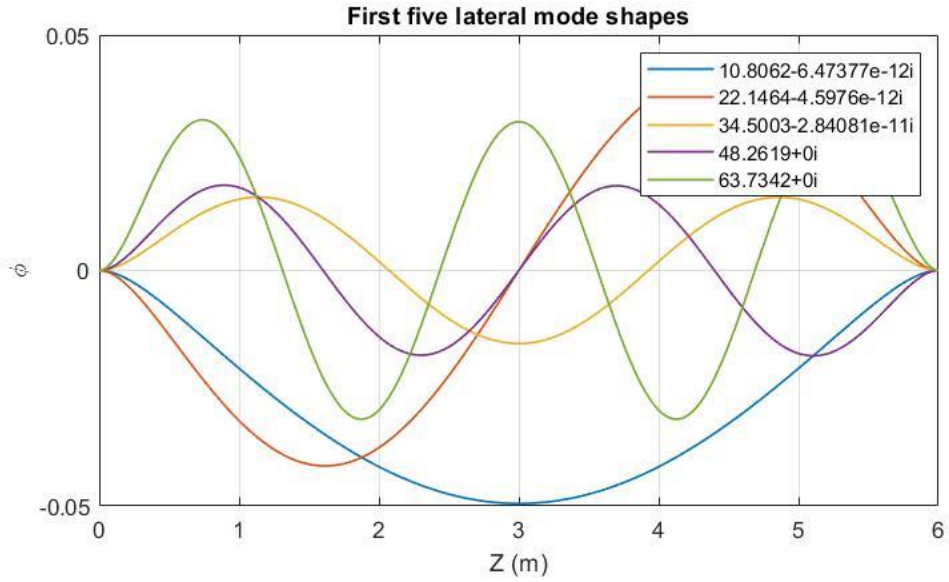


Figure 4-10 _ The first five modes in lateral direction

According the figures (4.5) to (4.10), the modes in lateral direction (Y-axis) are identical to those in vertical direction (X-axis) and that is because the beam element is axisymmetric, prismatic homogeneous.

Table 4.3 _ Natural frequency values (Hz)

First mode (Hz)	Second mode (Hz)	Third mode (Hz)	Forth mode (Hz)	Fifth mode (Hz)
10.8062	22.1464	34.5003	48.2619	63.7342

4.4 Dynamic responses of the system

The equation of motion which represents the dynamic behavior of the system is:

$$\mathbf{M}_T \ddot{\mathbf{q}} + \mathbf{C}_T \dot{\mathbf{q}} + \mathbf{K}_T \mathbf{q} = \mathbf{f}(t) \quad (4.12)$$

In which the proportional damping effect is considered:

$$\mathbf{C}_T = \alpha \mathbf{M}_T + \beta \mathbf{K}_T \quad (4.13)$$

To introduce the effect of damping in the system response, setting parameters α and β different from zero is necessary. In consideration of this, and taking into consideration the literature, our dynamic simulations have been performed with $\alpha = 0$ and $\beta = 1e^{-4}$.

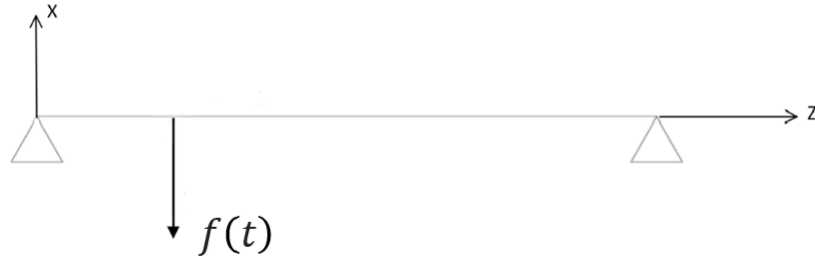
The dynamic study is performed in a discrete time manner, and in this regard, the time step is set $dt = 0.5e^{-3}s$.

With respect to time integration, as it was discussed earlier, Newmark scheme is adopted. Since the study of the dynamic behavior of the system is performed with respect to static equilibrium, as the initial condition to the Newmark method $\mathbf{q}_0, \dot{\mathbf{q}}_0$, are set as follow:

$$\mathbf{q}_0 = \mathbf{q}_s \quad \& \quad \dot{\mathbf{q}}_0 = \{\mathbf{0}\}$$

In which \mathbf{q}_s is the static equilibrium obtained by equation 4.8

4.4.1 Step Response



In this case, the excitation load is a step function along with the negative sign of the X-axis, which acts on the system at $t = 0s$ and vanishes at time $t = 2s$ as below:

$$f(t) = \begin{cases} 0, & t < 0 \\ F_0, & 0 \leq t \leq 2 \\ 0, & t \geq 2 \end{cases}$$

In which $F_0 = -20 \text{ kN}$. The load is applied on a node that is at the distance of 4 meters from the left end side constraint of the cable with respect to the coordinate Z .

The nodal force vector of the node which is subjected to the load would be expressed as the following vector:

$$f_n = \{0 \quad f(t) \quad 0 \quad 0 \quad 0 \quad 0\}$$

Step excitation is like an act of changing the static equilibrium to a new one at time t , and the response is a kind of transient free response about the new equilibrium condition. The case of study is a cable with a length of 6 meters and a diameter of 3.2 mm.

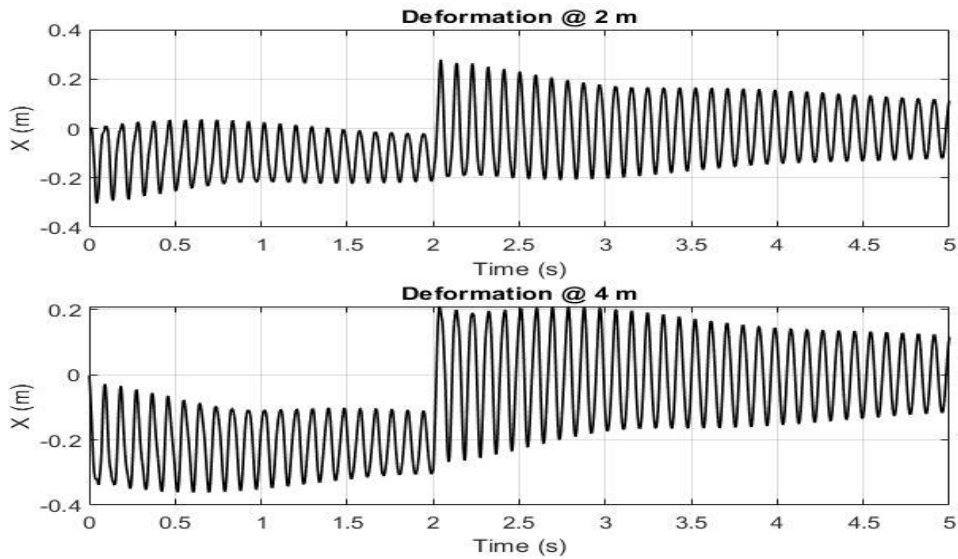


Figure 4-11 _ The response of the system to step function respectively at $z = 2m$ and $z = 4m$

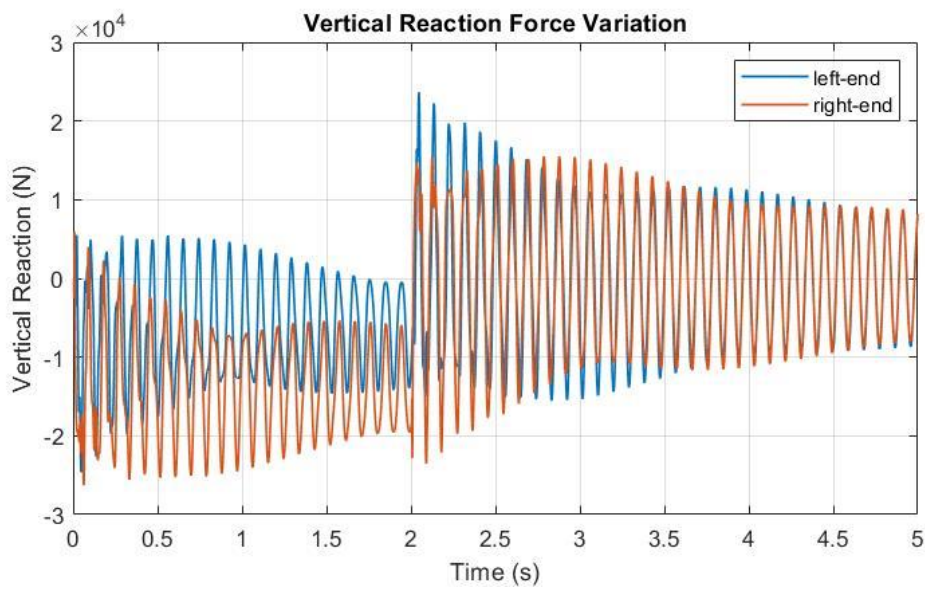
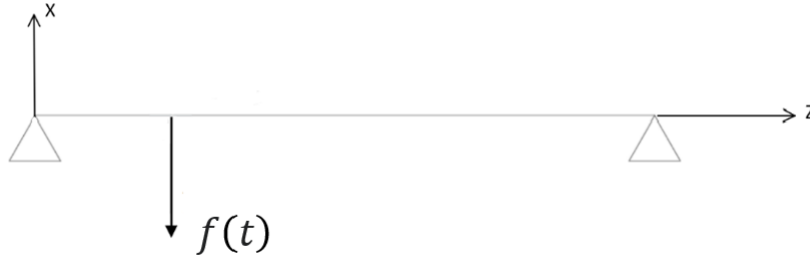


Figure 4-12 _ The vertical reaction forces of the constraints

Figure .12 depicts the time history of displacements of two points which are located at $Z = 2m$ and $Z = 4m$ and the load is applied on the latter one. As well as figure 4.13 displays the time history of variation of the constraint reaction alongside the vertical direction.

4.4.2 Harmonic Response



To study the harmonic response of the system, the system is excited by a harmonic load acting on a specific node that is at the distance of 4 meters from the left end side constraint of the cable with respect to the coordinate Z .

$$f(t) = F_0 \sin(2\pi\bar{f}t)$$

In which $F_0 = -20 \text{ kN}$, and to prevent possible confusion with nodal force vector \mathbf{f} , here the frequency in Hz is referred to as \bar{f} and the angular frequency is $\omega = 2\pi\bar{f}$.

As what mentioned earlier, the nodal force vector of the node which is subjected to the load would be expressed as the following vector:

$$\mathbf{f}_n = \{0 \quad f(t) \quad 0 \quad 0 \quad 0 \quad 0\}$$

The first natural frequency of the system is $\bar{f}_1 = 10.8062 \text{ Hz}$, and the frequency of the harmonic load is set close to it, $\bar{f} = 10 \text{ Hz}$.

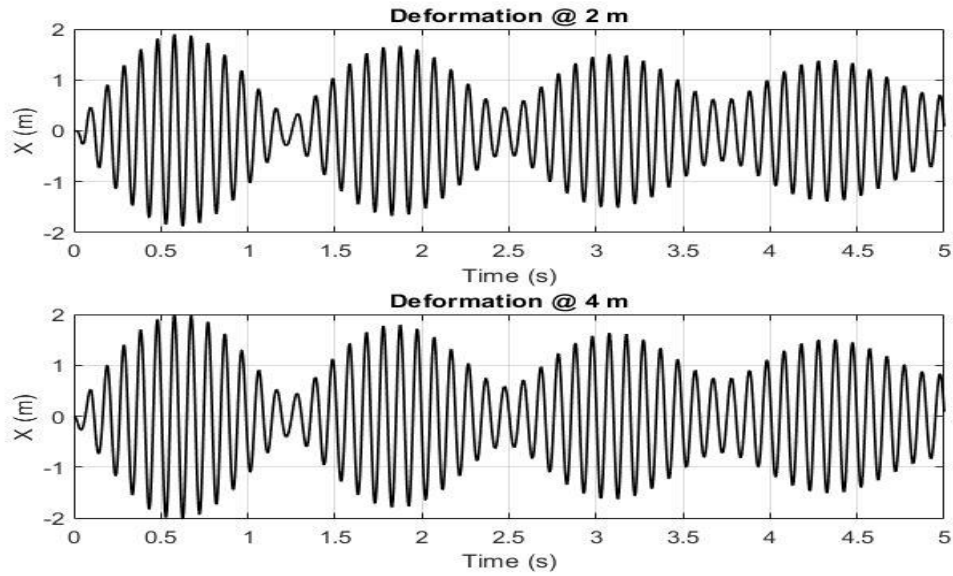


Figure 4-13 _ Harmonic response of the system at two points

Since the frequency of excitation is close the natural frequency, the so-called beating effect occurs which can be noticed in figure 4.14 displaying the time history of displacements of two nodes of the cable at $Z = 2m$ and $Z = 4m$.

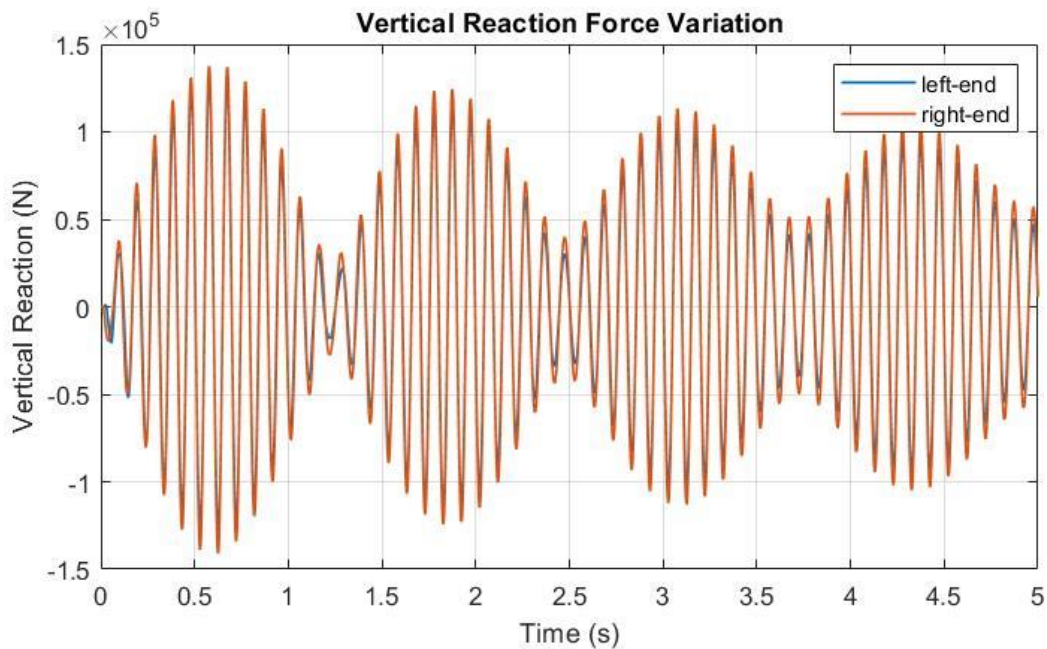


Figure 4-14 _ The vertical reaction forces of the constraints due to harmonic excitation

4.4.3 Response to moving load

The first challenge to simulate a ropeway is to model a moving load as representative to the cabin passage over the cable. A moving ropeway carrying cabins attached to it, can be modeled by considering a fixed and stationary cable subjected to a moving load. The load amplitude is $F_0 = -20 \text{ kN}$, and the speed of the load is $v_0 = 2 \text{ m/s}$.

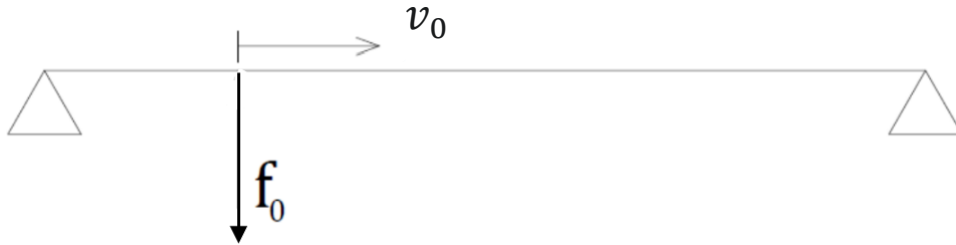


Figure 4-15 _ Scheme of the system under analysis

In this case, a very important point to consider is that since the load position changes in each time increment, as a result, in order to have a smooth movement of load through the entire cable and not only on the nodes, it is possible to consider the distribution of the load on each element using shape function matrix $[N]$ which is a function of space ($\zeta = \frac{z}{l}$).

$$\mathbf{f}_n = [N]^T \mathbf{f}_0 \quad (4.14)$$

With respect to Euler-Bernoulli beam element, the shape function matrix is:

$$[N] = \begin{bmatrix} N_{a1} & 0 & 0 & 0 & 0 & 0 & N_{a2} & 0 & 0 & 0 & 0 & 0 \\ 0 & N_{f_{1,1}} & 0 & 0 & 0 & N_{f_{1,2}} & 0 & N_{f_{1,3}} & 0 & 0 & 0 & N_{f_{1,4}} \\ 0 & 0 & N_{f_{1,1}} & 0 & -N_{f_{1,2}} & 0 & 0 & 0 & N_{f_{1,3}} & 0 & -N_{f_{1,4}} & 0 \\ 0 & 0 & 0 & N_{t1} & 0 & 0 & 0 & 0 & 0 & N_{t2} & 0 & 0 \\ 0 & 0 & -N_{f_{2,1}} & 0 & N_{f_{2,2}} & 0 & 0 & 0 & -N_{f_{2,3}} & 0 & N_{f_{2,4}} & 0 \\ 0 & N_{f_{2,1}} & 0 & 0 & 0 & N_{f_{2,2}} & 0 & N_{f_{2,3}} & 0 & 0 & 0 & N_{f_{2,4}} \end{bmatrix}$$

In which $N_a, N_f,$ and N_t are elements of shape function matrices in respectively axial, flexural, and torsional behavior which are already introduced on chapter 3.1.1, and they are functions of $(\zeta = \frac{z}{l})$.

At each time increment dt , these shape functions must be evaluated at the exact position at time t where the load is located. In this regard, the value is substituted:

$$z = v_0 t \quad \rightarrow \quad \zeta = \frac{v_0 t}{l}$$

In the equation (4.14).

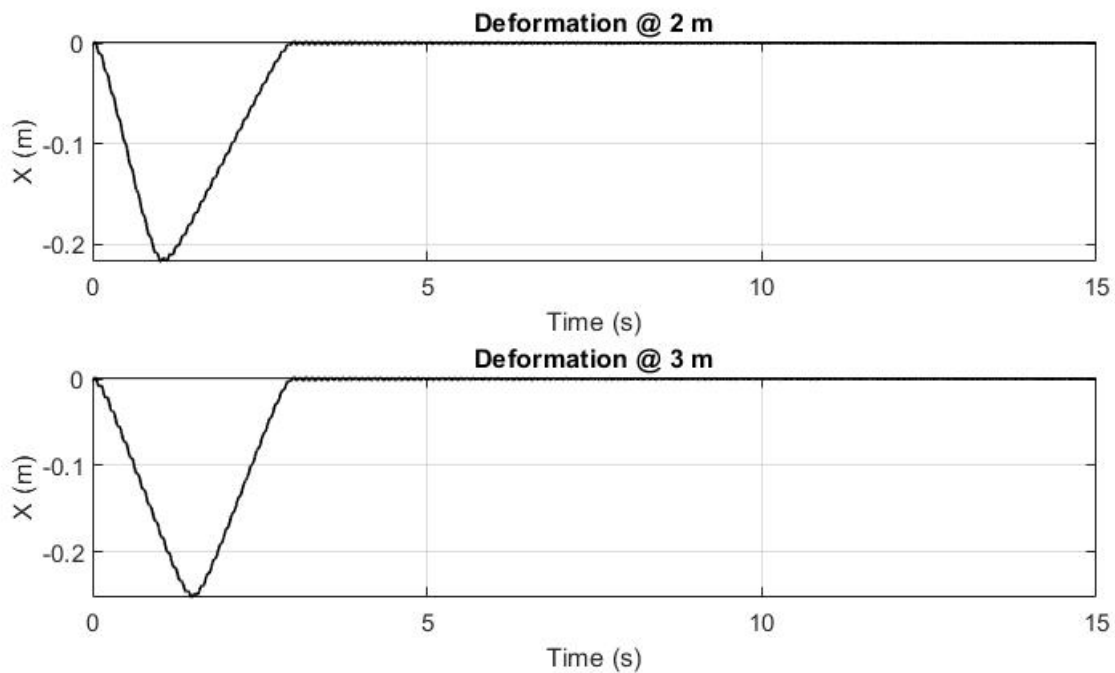


Figure 4-16 _ Time history of displacement at two points

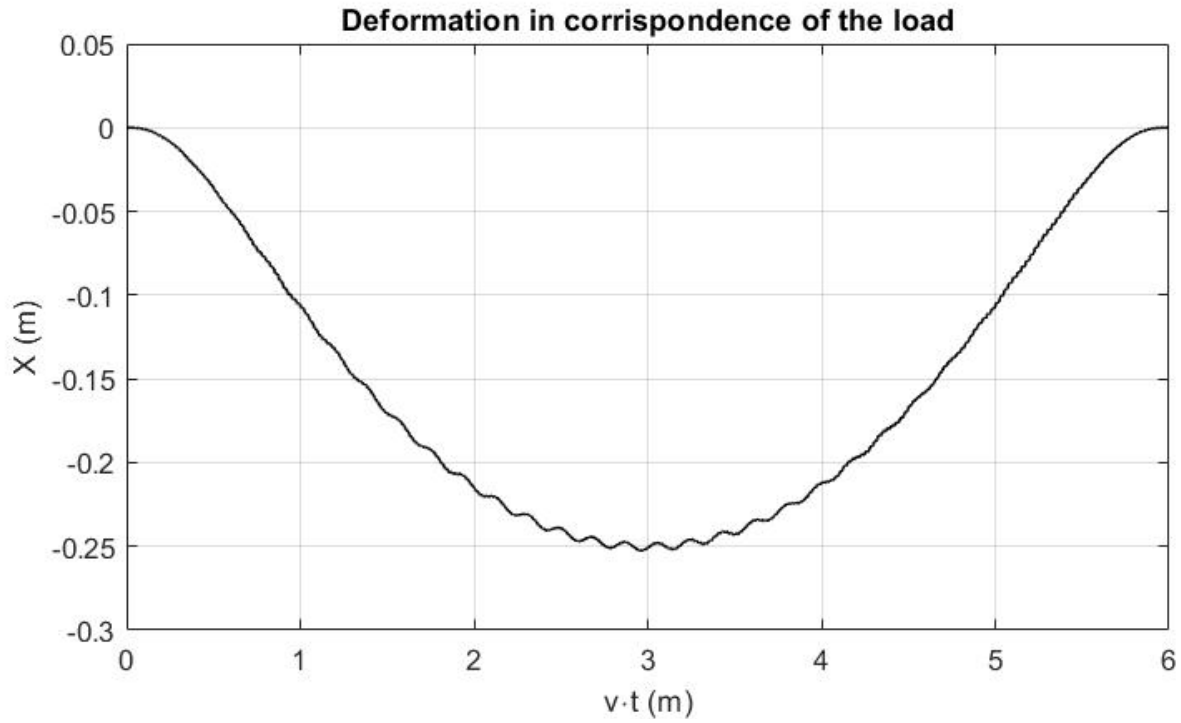


Figure 4-17 _ Deformation of the cable in the position under the load

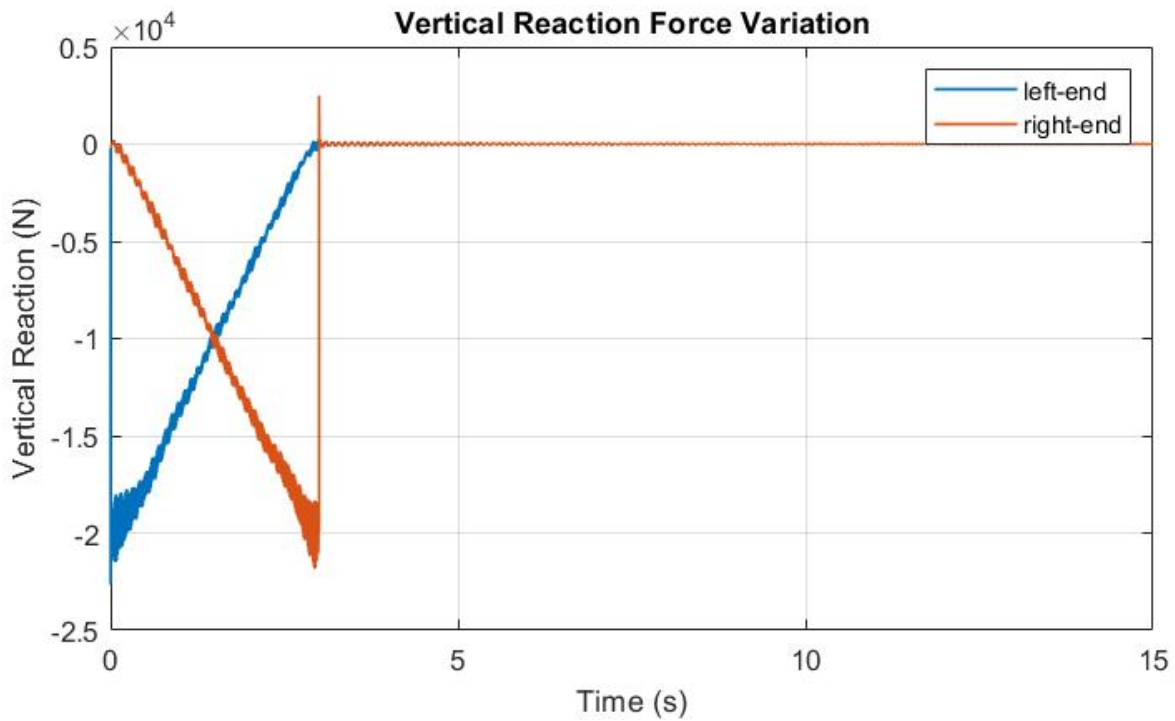


Figure 4-18 _ The variation of the vertical reaction forces over time

Considering a time integration intervals five time larger than what it takes for load to pass through the entire span, i.e. $0 \leq t \leq 5L/v_0$, analyzing also the transient deformation of the cable toward the static equilibrium after the load reaches the ending point is possible.

Figure (4.17) projects the time history of the displacements for two points over the cable, with respect to the coordinate Z , respectively at 2, *and* 3 meters from the constraint at the left end side. As the load passage is initiated over the cable, the cable starts to deform, and the aforementioned nodes move below so that they reach their maximum position at the time when the load is exactly hitting them. Afterward, as the load takes over the locations of the nodes, they move back towards their previous static location. Right after the load reaches the ending point, the cable displays an oscillatory behavior over the static configuration. Eventually, this transient response vanishes, and the cable settles on its static configuration.

5 2nd Configuration: Multi-Span cable

The discretized Euler-Bernoulli beam element and the Newmark scheme have been used successfully to model single-span beam. As the further step of this work, multi-span cable has been simulated similarly as single-span one adopting the same schemes for discretization and time integration. The simulation is initiated with a two-span beam with the following information:

Table 5.1 _ Geometrical data and parameters of the system

Density	$\rho = 8940 \frac{kg}{m^3}$	mass per unit of length $\mu = \rho \times \pi R^2 = 7.19 \frac{kg}{m}$
Elastic modulus	$E = 120 \times 10^9 \text{ Pa}$	Span length 1 $l = 10 \text{ m}$
Diameter	$D = 32 \times 10^{-3} \text{ m}$	Span length 2 $l = 8 \text{ m}$

5.1 Implementation of E-B element,

5.1.1 From local to global reference frame and rotation matrices

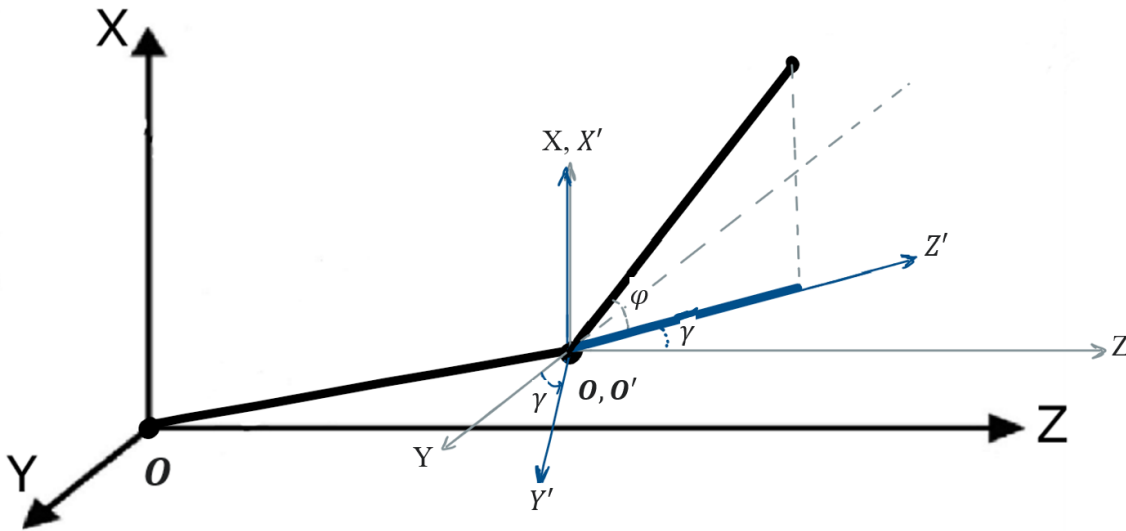


Figure 5-1 _ General orientation of beam in space

In figure 5.1, a two-span beam with general orientations in space is displayed. In this case, similarly, the global reference of frame O (XYZ) is defined so that the gravity field is directed toward the negative sign of the X-axis and the first span of the beam is in the XZ plane.

On the second beam, an intermediate reference frame O' ($X'Y'Z'$) is introduced so that the beam locates on the $X'Z'$ plane of the frame O' , and the X' -axis of frame O' has the same direction as X-axis in the O frame. In this way, the beam has an inclination of angle φ with respect to axis Y' and angle γ with respect to axis X. This logic will help us to drive the equation of motion of the beam with respect to the global reference frame using an adequate two-step transformation equation.

To link the displacement vectors q_{i_g} and q_{i_l} which are respectively the displacement vector of the i th node with respect to the global and local reference frames, first we need to introduce a coordinate transformation from intermediate frame to local one, and then from global to intermediate reference frame. Considering the fact that the local reference frame is the one with respect to which, the matrices are derived and the z – axis coincides with the axial direction of the beam.

1st: Transformation from intermediate reference frame O' to the local one:

$$\mathbf{R}_\varphi = \begin{bmatrix} \cos \varphi & \sin \varphi & 0 \\ -\sin \varphi & \cos \varphi & 0 \\ 0 & 0 & 1 \end{bmatrix}$$

The corresponding transformation can be expressed as:

$$\mathbf{q}_{i_l} = \mathbf{R}_\varphi \mathbf{q}_{i_{int}} \quad (5.1)$$

2nd: Transformation from global reference frame O to the intermediate one O' :

$$\mathbf{R}_\gamma = \begin{bmatrix} \cos \gamma & 0 & -\sin \gamma \\ 0 & 1 & 0 \\ \sin \gamma & 0 & \cos \gamma \end{bmatrix}$$

And the corresponding transformation can be expressed as:

$$\mathbf{q}_{i_{int}} = \mathbf{R}_\gamma \mathbf{q}_{i_g} \quad (5.2)$$

As a result, the direct transformation from global to local reference frame is conducted by the following rotation matrix and transformation expression:

$$\mathbf{R} = \mathbf{R}_\varphi \times \mathbf{R}_\gamma \quad \rightarrow \quad \mathbf{q}_{i_l} = \mathbf{R} \mathbf{q}_{i_g} \quad (5.3)$$

Again, the expanded rotation matrix \mathbf{R}' would be:

$$\mathbf{R}' = \begin{bmatrix} [\mathbf{R}_{3 \times 3}] & [\mathbf{0}_{3 \times 3}] & [\mathbf{0}_{3 \times 3}] & [\mathbf{0}_{3 \times 3}] \\ [\mathbf{0}_{3 \times 3}] & [\mathbf{R}_{3 \times 3}] & [\mathbf{0}_{3 \times 3}] & [\mathbf{0}_{3 \times 3}] \\ [\mathbf{0}_{3 \times 3}] & [\mathbf{0}_{3 \times 3}] & [\mathbf{R}_{3 \times 3}] & [\mathbf{0}_{3 \times 3}] \\ [\mathbf{0}_{3 \times 3}] & [\mathbf{0}_{3 \times 3}] & [\mathbf{0}_{3 \times 3}] & [\mathbf{R}_{3 \times 3}] \end{bmatrix}_{12 \times 12}$$

As what we have seen in section 4.1.2, the equation of the motion with respect to the global reference frame is:

$$\mathbf{R}'^T \mathbf{M} \mathbf{R}' \ddot{\mathbf{q}}_g + \mathbf{R}'^T \mathbf{K} \mathbf{R}' \mathbf{q}_g = \mathbf{f}_g \quad (5.4)$$

And the global matrices and vector associated with one element is:

$$\begin{aligned} \mathbf{M}_g &= \mathbf{R}'^T \mathbf{M}_l \mathbf{R}' \\ \mathbf{K}_g &= \mathbf{R}'^T \mathbf{K}_l \mathbf{R}' \\ \mathbf{f}_g &= \mathbf{R}'^T \mathbf{f}_l \end{aligned} \quad (5.5)$$

5.1.2 Assembling and mapping matrices

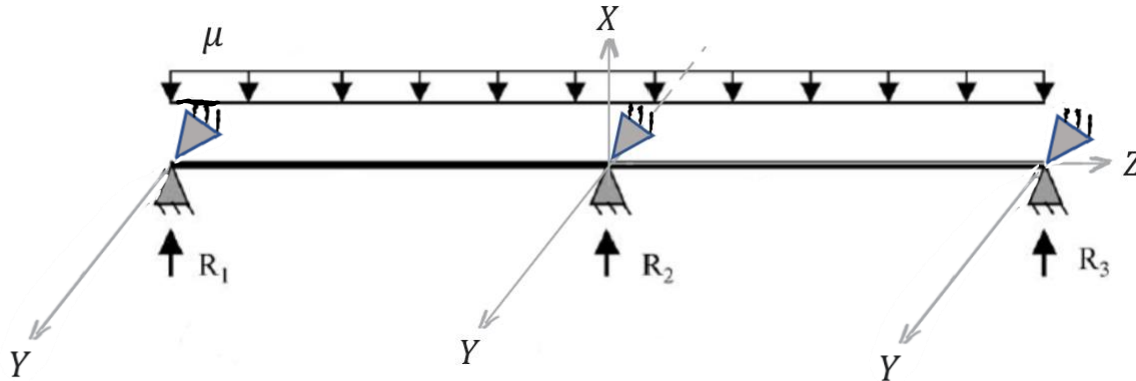


Figure 5-2 _ Two-span beam with one intermediate constraint

As it was discussed for one-span beam, procedure to assemble the elements of multi-span beam follow the same logic. After obtaining the global matrices and global nodal force vector, since all elements, displacements, and forces are expressed with respect to the same reference frame (global), the map matrix can be developed without considering the constraints at this stage.

$$\{q\} = \{u_{z1} \ u_{x1} \ u_{y1} \ \theta_{z1} \ \theta_{x1} \ \theta_{y1} \ \dots \ u_{z4} \ u_{x4} \ u_{y4} \ \theta_{z4} \ \theta_{x4} \ \theta_{y4}\}'_{1 \times 24}$$

Table 5.2 _ Assembling table

	u_{z1}	u_{x1}	u_{y1}	θ_{z1}	θ_{x1}	θ_{y1}	u_{z2}	u_{x2}	u_{y2}	θ_{z2}	θ_{x2}	θ_{y2}	u_{z3}	u_{x3}	u_{y3}	θ_{z3}	θ_{x3}	θ_{y3}	...	θ_{x4}	θ_{y4}
1	1	2	3	4	5	6	7	8	9	10	11	12							...		
2							1	2	3	3	4	5	6	7	8	9	10	11	...		
3													1	2	3	4	5	6	...	11	12

Once the mapping is done the global mass and stiffness matrices will be of the structure as what we have seen in single-span beam.

the global equation of motion of the entire structure with proportional damping is:

$$\mathbf{M}_T \ddot{\mathbf{q}} + \mathbf{C}_T \dot{\mathbf{q}} + \mathbf{K}_T \mathbf{q} = \mathbf{f}_T(t) \quad (5.6)$$

5.2 Boundary Conditions and Static equilibrium

Within a multi-span beam, the intermediate support, in our case, which is usually a pulley on which the cable passes, constrains only the vertical and lateral degrees of freedom (u_{xi}, u_{yi}) on the node i which is in the surface contact of the pulley. As a result, the pulley can simply be modeled by adding only two strong translational stiffness (k_i, χ_i) at the corresponding DOFs within the global stiffness matrix of the whole structure.

Considering the same small example, we discussed in section 4.1.3, but this time, the third node is constrained by the pulley, with a similar boundary condition at left and right end sides. Therefore, the displacement vectors of the constraint nodes would be as:

$$\{q_1\} = \begin{Bmatrix} u_{z1} \\ u_{X1} \\ u_{Y1} \\ \theta_{z1} \\ \theta_{X1} \\ \theta_{Y1} \end{Bmatrix} = \begin{Bmatrix} 0 \\ 0 \\ 0 \\ 0 \\ 0 \\ 0 \end{Bmatrix}, \quad \{q_3\} = \begin{Bmatrix} u_{z3} \\ u_{X3} \\ u_{Y3} \\ \theta_{z3} \\ \theta_{X3} \\ \theta_{Y3} \end{Bmatrix} = \begin{Bmatrix} u_{z3} \\ 0 \\ 0 \\ \theta_{z3} \\ \theta_{X3} \\ \theta_{Y3} \end{Bmatrix}, \quad \{q_4\} = \begin{Bmatrix} u_{z1} \\ u_{X1} \\ u_{Y1} \\ \theta_{z1} \\ \theta_{X1} \\ \theta_{Y1} \end{Bmatrix} = \begin{Bmatrix} u_{z1} \\ 0 \\ 0 \\ 0 \\ 0 \\ 0 \end{Bmatrix}$$

Adopting the same solution, k and χ are the relevant stiffnesses that are to be added to global stiffness matrix implementing respectively on translational and rotational DOFs. The additional stiffnesses are as the following:

$$\{k_{z1} \ k_{X1} \ k_{Y1} \ \chi_{z1} \ \chi_{X1} \ \chi_{Y1} \ k_{X3} \ k_{Y3} \ k_{X4} \ k_{Y4} \ \chi_{z4} \ \chi_{X4} \ \chi_{Y4}\}$$

Incrementation of potential energy due to additional stiffnesses is:

$$\Delta U = \frac{1}{2}k_{z1}(u_{z1})^2 + \frac{1}{2}k_{x1}(u_{x1})^2 + \frac{1}{2}k_{y1}(u_{y1})^2 + \frac{1}{2}\chi_{z1}(\theta_{z1})^2 + \frac{1}{2}\chi_{x1}(\theta_{x1})^2 + \frac{1}{2}\chi_{y1}(\theta_{y1})^2 + \dots$$

$$\dots + \frac{1}{2}k_{x3}(u_{x3})^2 + \frac{1}{2}k_{y3}(u_{y3})^2 + \frac{1}{2}k_{x4}(u_{x4})^2 + \frac{1}{2}k_{y4}(u_{y4})^2 + \frac{1}{2}\chi_{z4}(\theta_{z4})^2 + \frac{1}{2}\chi_{x4}(\theta_{x4})^2 +$$

$$\dots + \frac{1}{2}\chi_{y4}(\theta_{y4})^2$$

$$\frac{d}{dt} \left(\frac{\partial \Delta U}{\partial u_{z1}} \right) = k_{z1} u_{z1}$$

$$\frac{d}{dt} \left(\frac{\partial \Delta U}{\partial u_{x4}} \right) = k_{x4} u_{x4}$$

$$\frac{d}{dt} \left(\frac{\partial \Delta U}{\partial u_{x1}} \right) = k_{x1} u_{x1}$$

$$\frac{d}{dt} \left(\frac{\partial \Delta U}{\partial u_{y4}} \right) = k_{y4} u_{y4}$$

$$\frac{d}{dt} \left(\frac{\partial \Delta U}{\partial u_{y1}} \right) = k_{y1} u_{y1}$$

$$\frac{d}{dt} \left(\frac{\partial \Delta U}{\partial \theta_{z4}} \right) = \chi_{z4} \theta_{z4}$$

$$\frac{d}{dt} \left(\frac{\partial \Delta U}{\partial \theta_{z1}} \right) = \chi_{z1} \theta_{z1}$$

$$\frac{d}{dt} \left(\frac{\partial \Delta U}{\partial \theta_{x4}} \right) = \chi_{x4} \theta_{x4}$$

$$\frac{d}{dt} \left(\frac{\partial \Delta U}{\partial \theta_{x1}} \right) = \chi_{x1} \theta_{x1}$$

$$\frac{d}{dt} \left(\frac{\partial \Delta U}{\partial \theta_{y4}} \right) = \chi_{y4} \theta_{y4}$$

$$\frac{d}{dt} \left(\frac{\partial \Delta U}{\partial \theta_{y1}} \right) = \chi_{y1} \theta_{y1}$$

$$\frac{d}{dt} \left(\frac{\partial \Delta U}{\partial u_{x3}} \right) = k_{x3} u_{x3}$$

$$\frac{d}{dt} \left(\frac{\partial \Delta U}{\partial u_{y3}} \right) = k_{y3} u_{y3}$$

$$\begin{bmatrix} \blacksquare + k_{z1} & \blacksquare & \blacksquare & \dots & 0 & 0 & \dots & 0 & 0 \\ \blacksquare & \blacksquare + k_{x1} & \blacksquare & \dots & 0 & 0 & \dots & 0 & 0 \\ \blacksquare & \blacksquare & \blacksquare + k_{y1} & \dots & 0 & 0 & \dots & 0 & 0 \\ \blacksquare & \blacksquare & \blacksquare & \ddots & \vdots & \vdots & \dots & 0 & 0 \\ \blacksquare & \blacksquare & \blacksquare & \dots & \blacksquare + \chi_{x3} & \blacksquare & \dots & 0 & 0 \\ \vdots & \vdots & \vdots & \vdots & \vdots & \blacksquare + \chi_{y3} & \dots & 0 & 0 \\ 0 & 0 & 0 & 0 & 0 & 0 & \dots & \blacksquare + \chi_{x4} & \blacksquare \\ 0 & 0 & 0 & 0 & 0 & 0 & \dots & \blacksquare & \blacksquare + \chi_{y4} \end{bmatrix} \begin{Bmatrix} u_{z1} \\ u_{x1} \\ u_{y1} \\ \vdots \\ u_{x3} \\ u_{y3} \\ \vdots \\ \theta_{x24} \\ \theta_{y24} \end{Bmatrix}$$

5.2.1 Calculation of Static equilibrium and Reaction Forces

The static displacement of the system due to the weight of the cable:

$$\mathbf{K}_T \mathbf{q}_s = \mathbf{f}_T \quad \rightarrow \quad \mathbf{q}_s = \mathbf{K}_T^{-1} \mathbf{f}_T \quad (5.7)$$

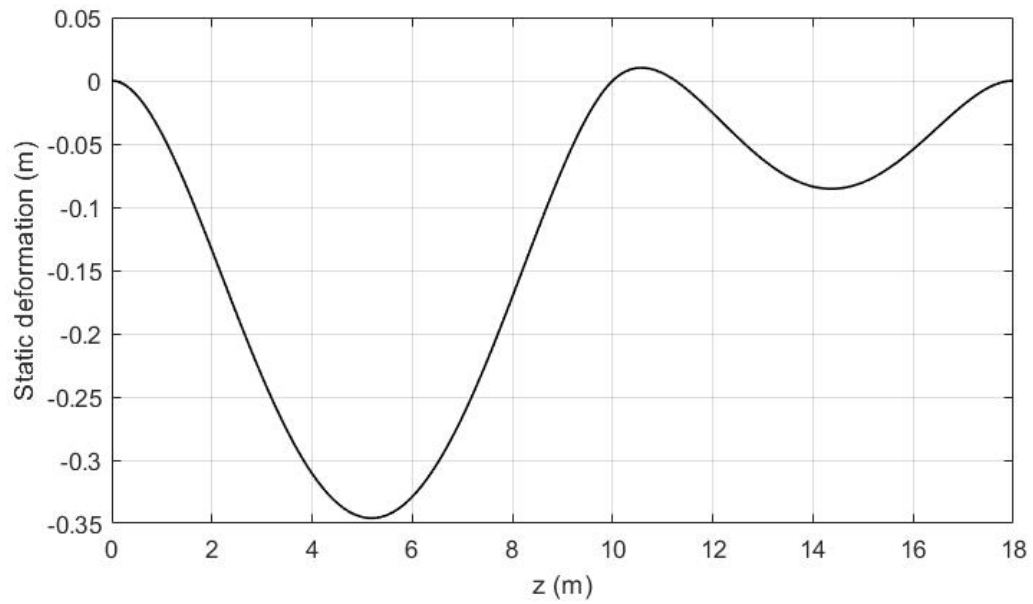


Figure 5-3 _ Static equilibrium

To calculate the reaction forces on pulley, we adopt the same logic used for boundary reaction forces

$$F_{z1} = k_{z1}u_{z1}$$

$$F_{X1} = k_{X1}u_{X1}$$

$$F_{Y1} = k_{Y1}u_{Y1}$$

$$M_{z1} = \chi_{z1}\theta_{z1}$$

$$M_{X1} = \chi_{X1}\theta_{X1}$$

$$M_{Y1} = \chi_{Y1}\theta_{Y1}$$

$$F_{X2} = k_{X2}u_{X2}$$

$$F_{Y2} = k_{Y2}u_{Y2}$$

$$M_{z2} = \chi_{z2}\theta_{z2}$$

$$M_{X2} = \chi_{X2}\theta_{X2}$$

$$M_{Y2} = \chi_{Y2}\theta_{Y2}$$

$$F_{X3} = k_{X3}u_{X3}$$

$$F_{Y3} = k_{Y3}u_{Y3}$$

5.3 Modal analysis of the system and validation

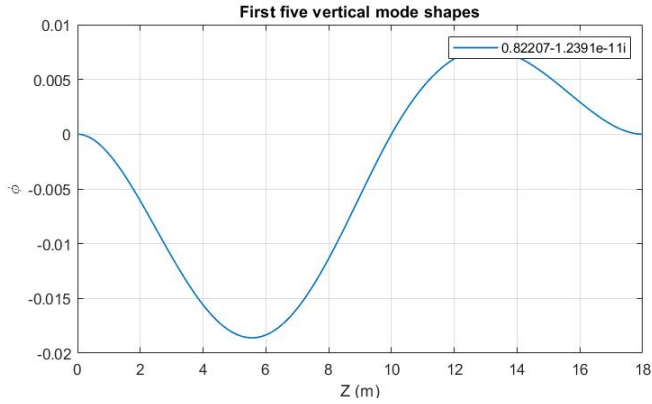


Figure 5-4 _ The 1st vertical mode, $T = 0$

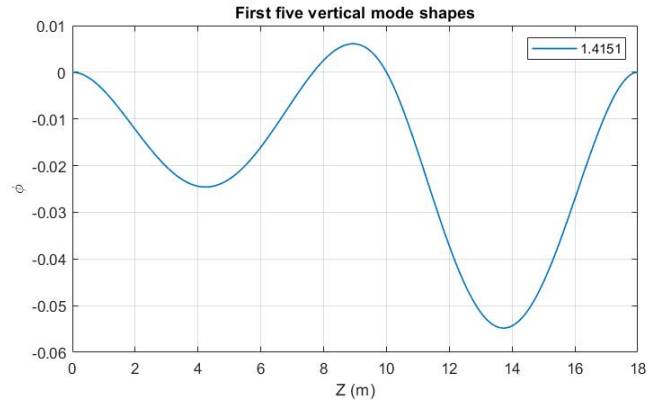


Figure 5-5 _ The 2nd vertical mode, $T = 0$

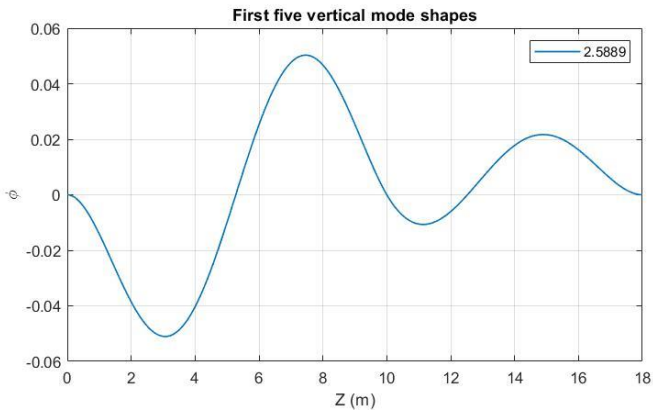


Figure 5-6 _ The 3rd vertical mode, $T=0$

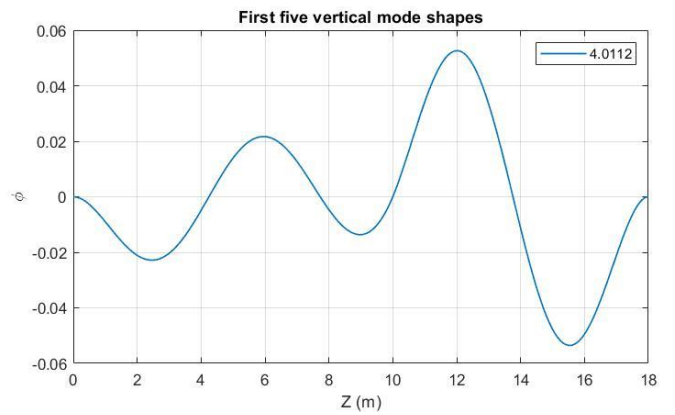


Figure 5-7 _ The 4th vertical mode, $T=0$

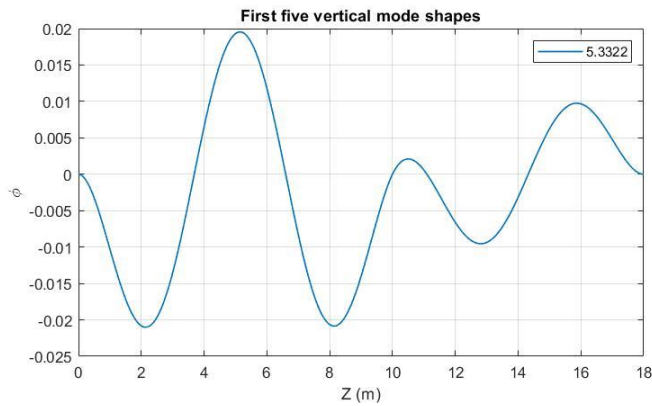


Figure 5-8 _ The 5th vertical mode, $T=0$

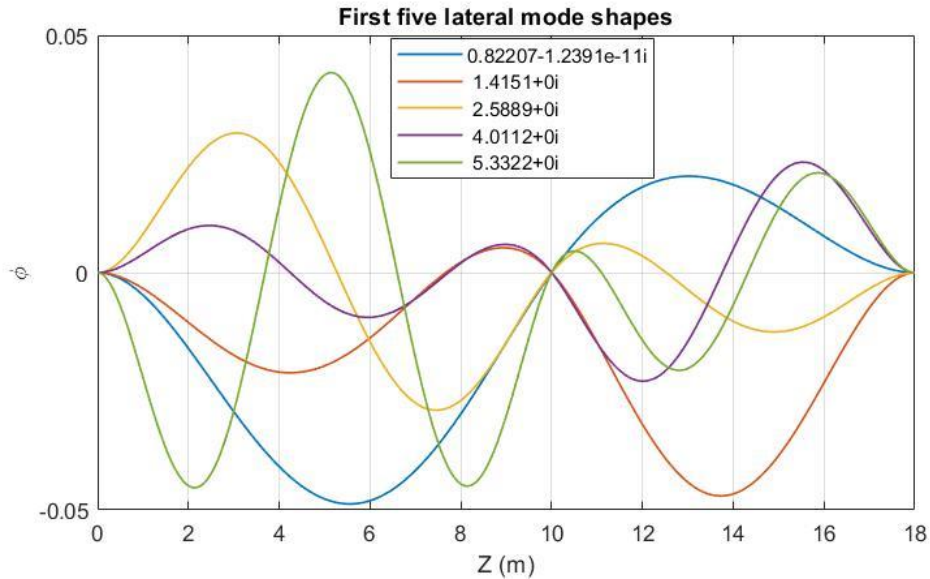


Figure 5-9 -The first five modes in lateral direction

As we set the pretension T equal to zero, we would not have anymore stiffening effect caused by axial load, therefore the range of frequencies are low. According to the different validation which have performed, these are promising and reliable.

Table 5.3 _ Natural frequency values (Hz)

First mode (Hz)	Second mode (Hz)	Third mode (Hz)	Forth mode (Hz)	Fifth mode (Hz)
0.82207	1.4151	2.5889	4.0112	5.3322

These mode shapes so far, are related to the multi-span cable without any pretension. The modal shapes of multi-span cable under pretension, by adopting equation (3.9), with respect to two values of tensile force as $T = 20kN$ and $T = 100kN$ are presented below:

Modals of multi-span cable subjected to tensile load $T = 20kN$:

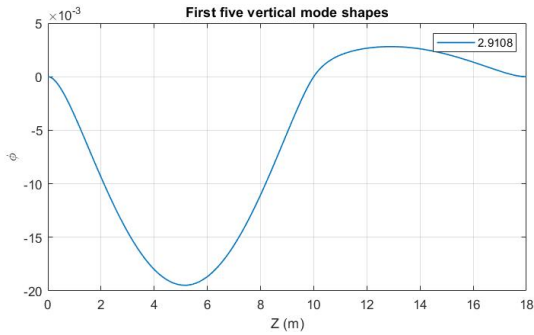


Figure 5-10 _ The 1st vertical mode, $T=20kN$

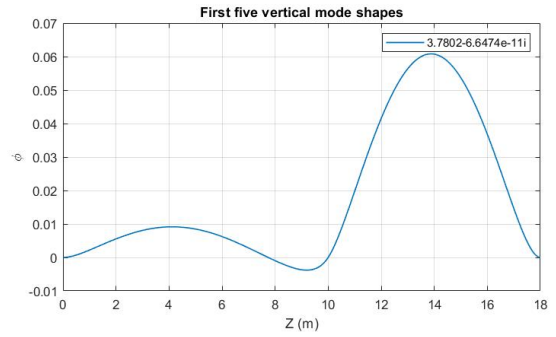


Figure 5-11 _ The 2nd vertical mode, $T=20kN$

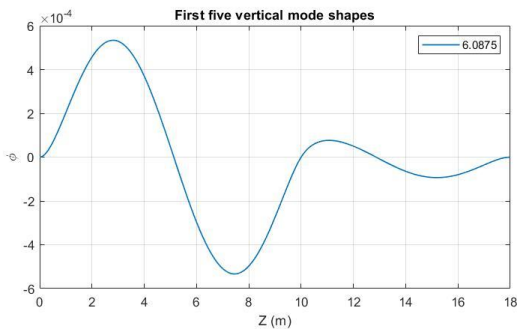


Figure 5-12 _ The 3rd vertical mode, $T=20kN$

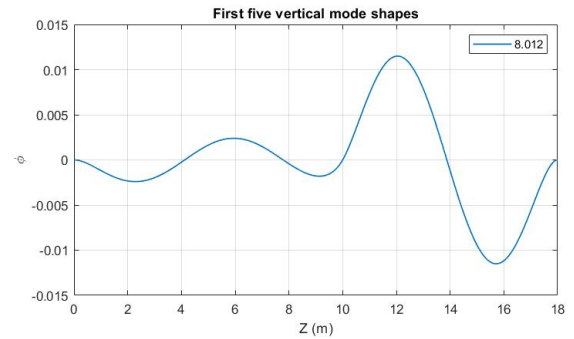


Figure 5-13 _ The 4th vertical mode, $T=20kN$

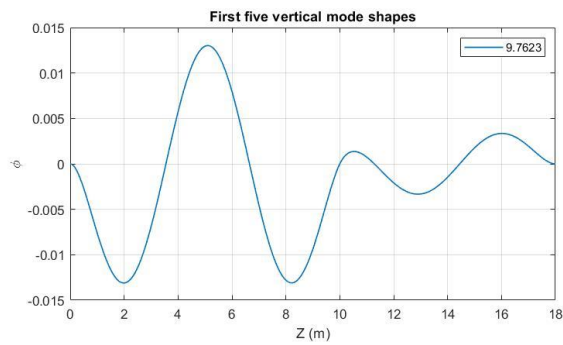


Figure 5-14 _ The 5th vertical mode, $T=20kN$

Modals of multi-span cable subjected to tensile load $T = 100\text{kN}$:

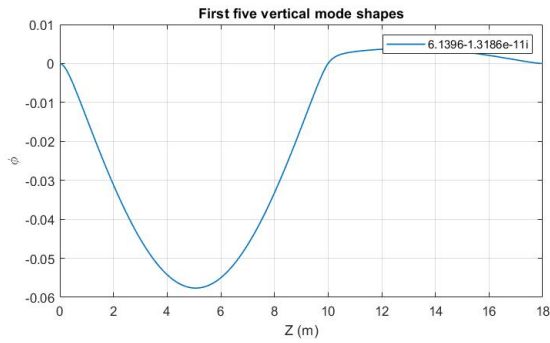


Figure 5-15 _ The 1st vertical mode, $T=100\text{kN}$

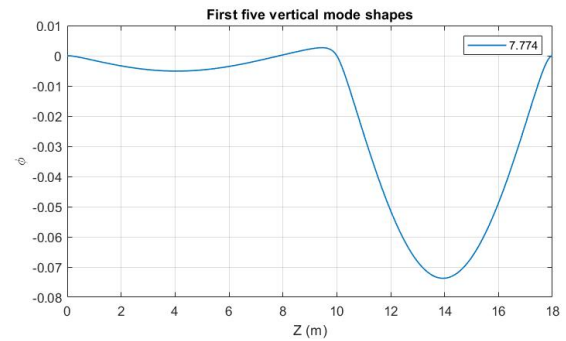


Figure 5-16 _ The 2nd vertical mode, $T=100\text{kN}$

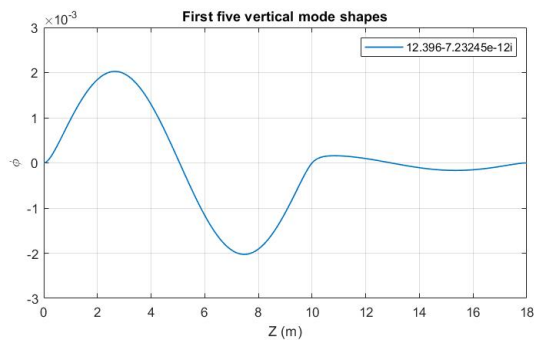


Figure 5-17 _ The 3rd vertical mode, $T=100\text{kN}$

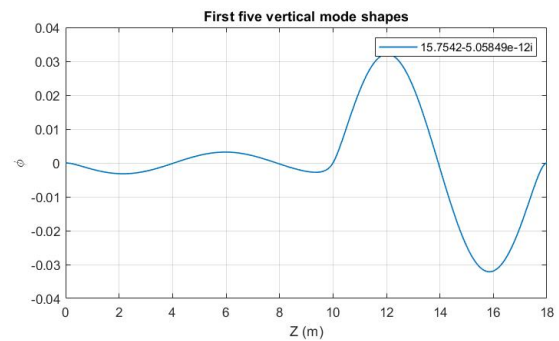


Figure 5-18 _ The 4th vertical mode, $T=100\text{kN}$

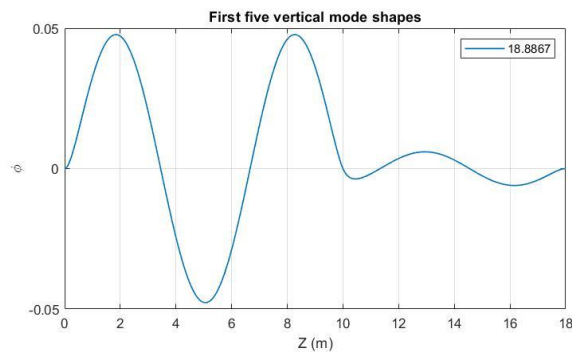


Figure 5-19 _ The 5th vertical mode, $T=100\text{kN}$

According to the mode shapes regarding cases $T = 20kN$ and $T = 100kN$, apparently the method adopted to introduce the pretension in cable, in this specific configuration, caused an inconsistency. By increasing the tensile load on the cable, it can be observed that the two span's dynamics gets somehow more isolated from each other's which is not acceptable. This means the high value of axial pretension for slender beams causes difficulties for the geometric stiffness matrix to linearize properly the geometric nonlinearity caused by the axial pretension on the cable.

5.4 Dynamic responses of the system

To study the dynamic equation:

$$\mathbf{M}_T \ddot{\mathbf{q}} + \mathbf{C}_T \dot{\mathbf{q}} + \mathbf{K}_T \mathbf{q} = \mathbf{f}_T(t) \quad (5.8)$$

With proportional damping parameters α and β the same as previous case of study, respectively 0 and $\frac{1}{4}$, the same consideration about initial conditions q_0, \dot{q}_0 , time step dt , and time integration scheme have been adopted:

$$\mathbf{q}_0 = \mathbf{q}_s \quad \& \quad \dot{\mathbf{q}}_0 = \{\mathbf{0}\} \quad \& \quad dt = 0.5e^{-3}s$$

5.4.1 Step Response

The same step function excites the system acting on a node located at $z = 7m$ starting at $t = 0$ and lasts for 2 seconds:

$$f(t) = \begin{cases} 0, & t < 0 \\ F_0, & 0 \leq t \leq 2 \\ 0, & t \geq 2 \end{cases} \quad \& \quad F_0 = -2 \text{ kN}$$

The nodal force vector of the node which is subjected to the load:

$$\mathbf{f}_n = \{0 \quad f(t) \quad 0 \quad 0 \quad 0 \quad 0\}$$

Results

In figure 5.11, time history of the displacement of two nodes (one node at each span) is depicted, and figure 5.12, displays the reaction forces due to step response of the system.

The natural frequencies are low, and since step response is kind of free response over new equilibrium, we can see the response takes place at a very low speed over time.

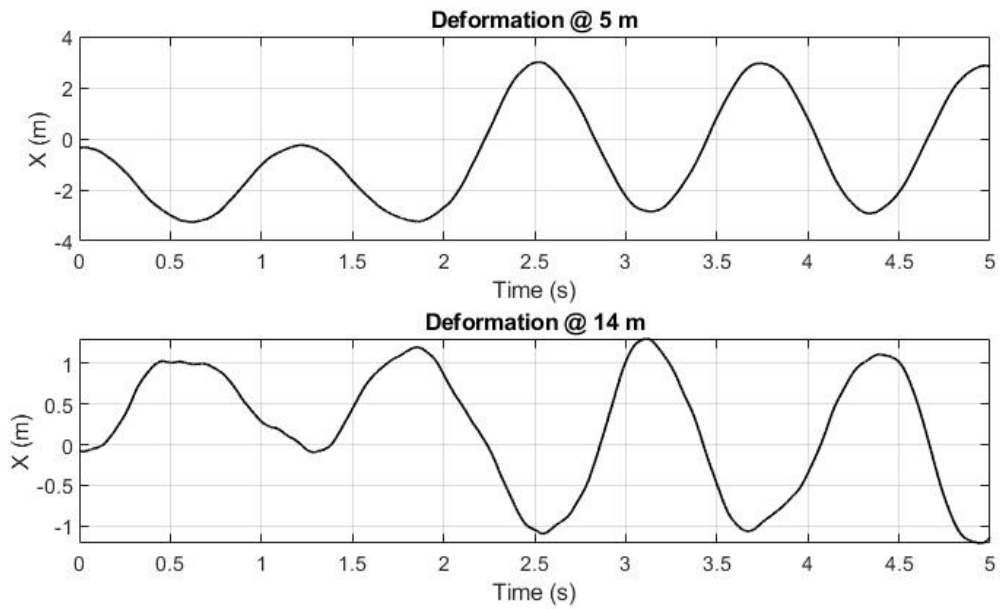


Figure 5-20 _ Step response of two nodes at 5m & 14m

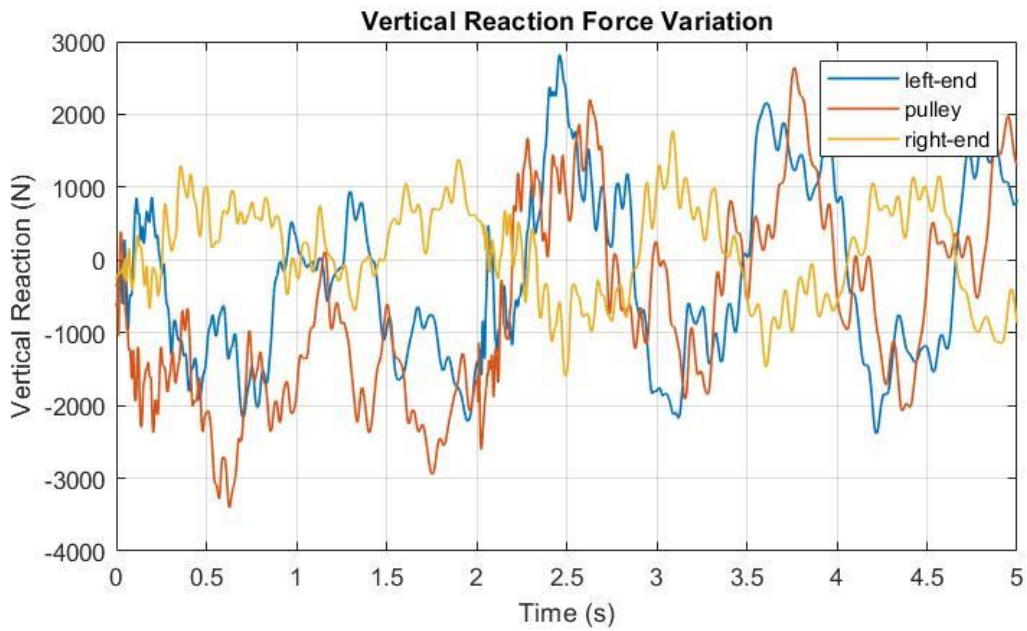


Figure 5-21 _ Variation of reaction forces over time

5.4.2 Harmonic Response

Here the aim is to study of the two-span beam response to a harmonic load with frequency $\bar{f} = 1 \text{ Hz}$ (close to first natural frequency).

$$f(t) = F_0 \sin(2\pi\bar{f}t) \quad \& \quad F_0 = -2 \text{ kN}$$

The nodal force vector of the node on which the load acts:

$$\mathbf{f}_n = \{0 \quad f(t) \quad 0 \quad 0 \quad 0 \quad 0\}$$

The first natural frequency of the system is $\bar{f}_1 = 0.82207 \text{ Hz}$, and the frequency of the harmonic load is set close to it, $\bar{f} = 1 \text{ Hz}$. Since the exciting frequency is close to one of the natural frequencies beating kind of behavior can be detected. The load is applied on a node at $z = 4 \text{ m}$.

Result

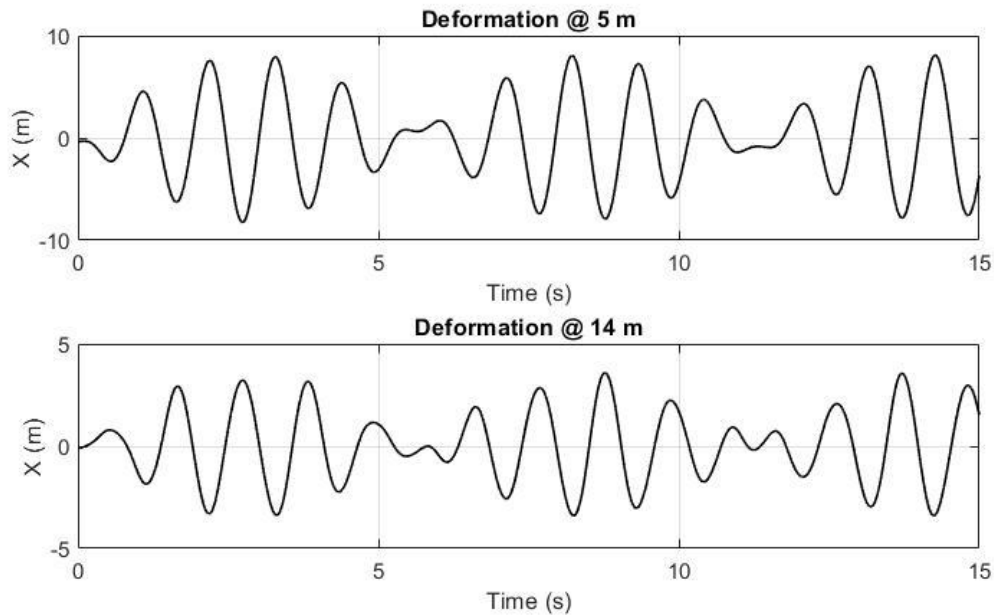


Figure 5-22 _ Harmonic response of two nodes at 5m & 14m

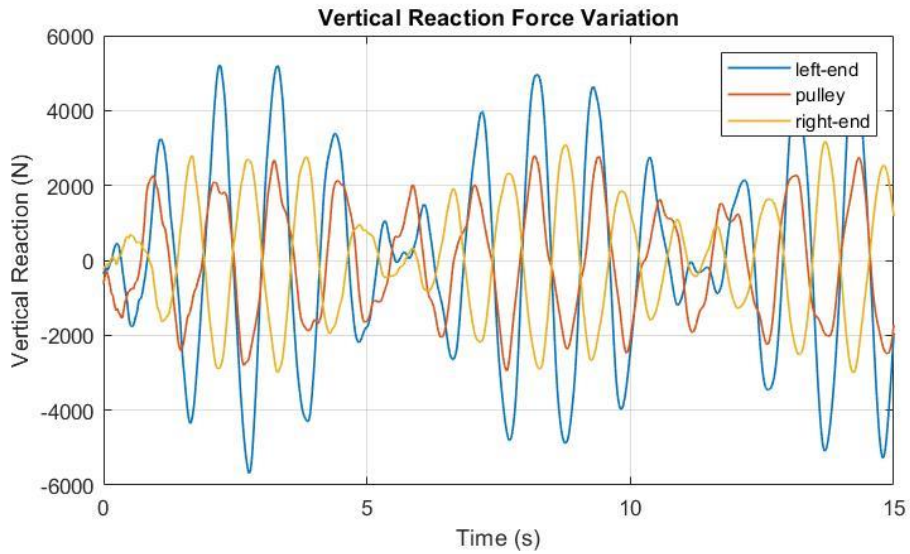


Figure 5-23 _ Variation of reaction forces over time

5.4.3 Response to moving load

This part follows the same logic as what was considered in the section 4.4.3 with regards to response to moving of a single-span cable. In this case the amplitude of the load is $F_0 = -2 \text{ kN}$ and the cable is not subjected to any tensile force. The results in this configuration would be as below:

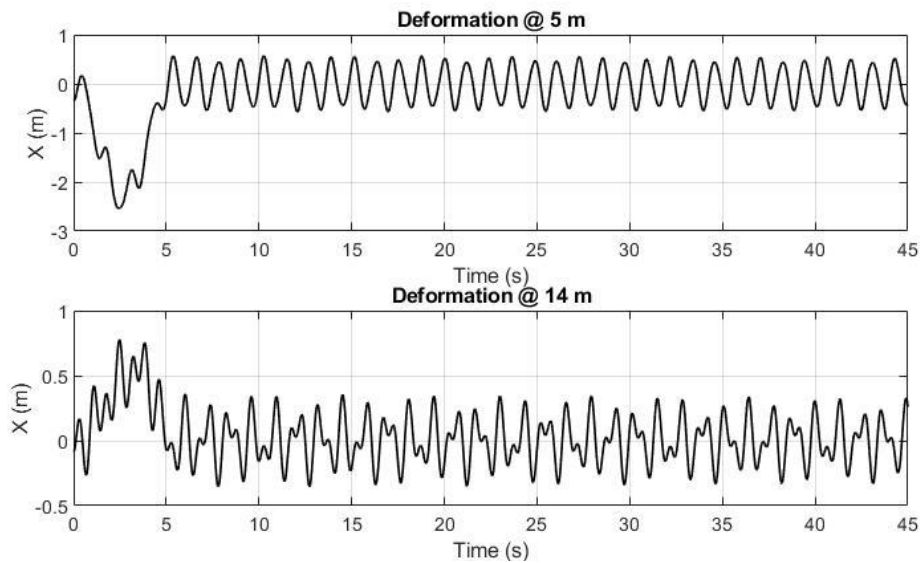


Figure 5-24 _ Time history of displacement at two points

In figure 5.24, the displacement of two points is displayed, the first point at $Z = 5$ is located at the middle of the first span and the second point at $Z = 14$ is the second span midpoint.

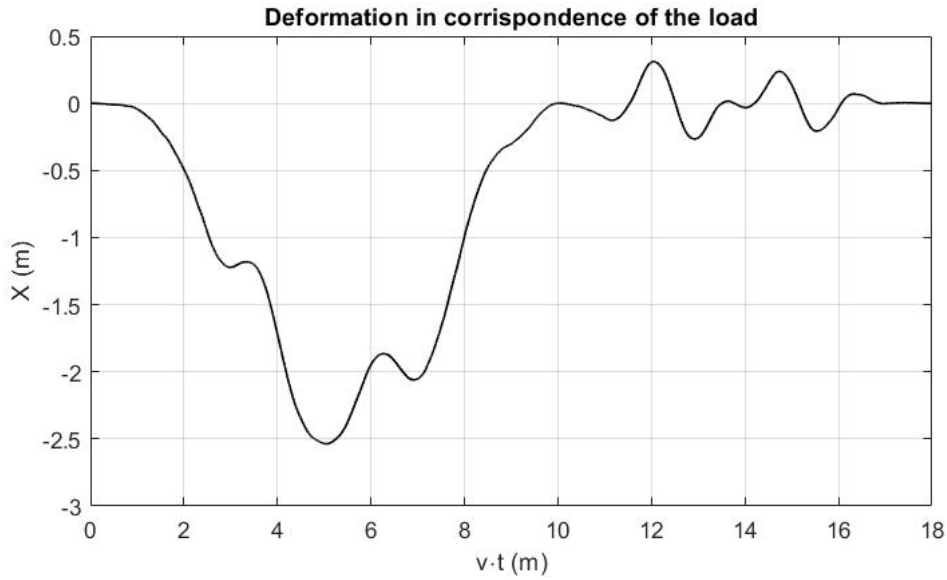


Figure 5-25 _ Deformation of the cable with correspondence of the load

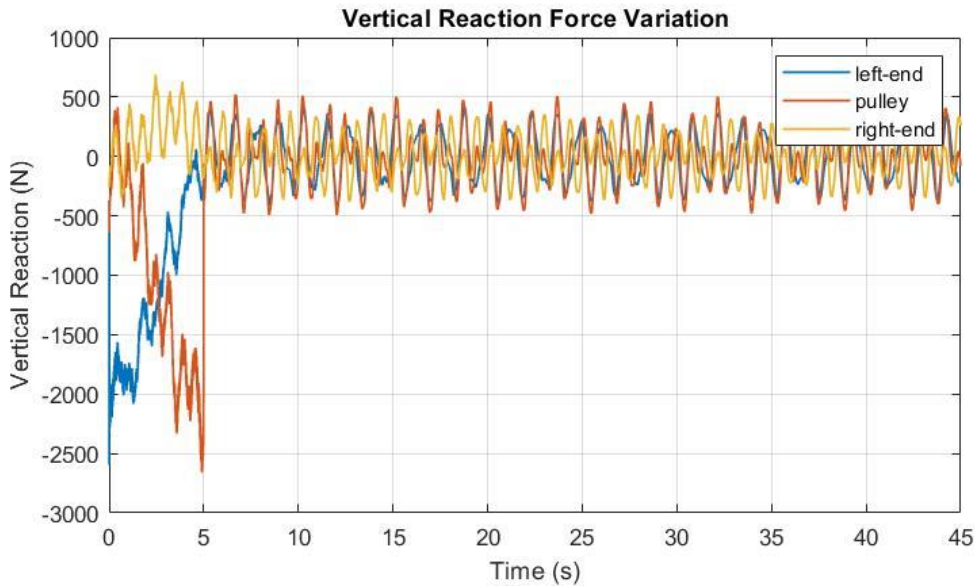


Figure 5-26 _ The variation of the vertical reaction forces over time

5.5 Sensitivity to the length of element

FE model is a very strong and powerful tool to model different systems, but it could be a very time-consuming computation. As a result, in order to minimize the required time for the process of calculation it is necessary to find the optimum length of the element to achieve reliable results while the time is saved. With respect to the harmonic response of the multi-span cable, for the elements of length larger than 5 cm the results start getting diverge. And this number for moving load on multi-span cable is 2.857 cm.

Hereafter, a comparison between element length has been performed for the harmonic response of multi-span beam:

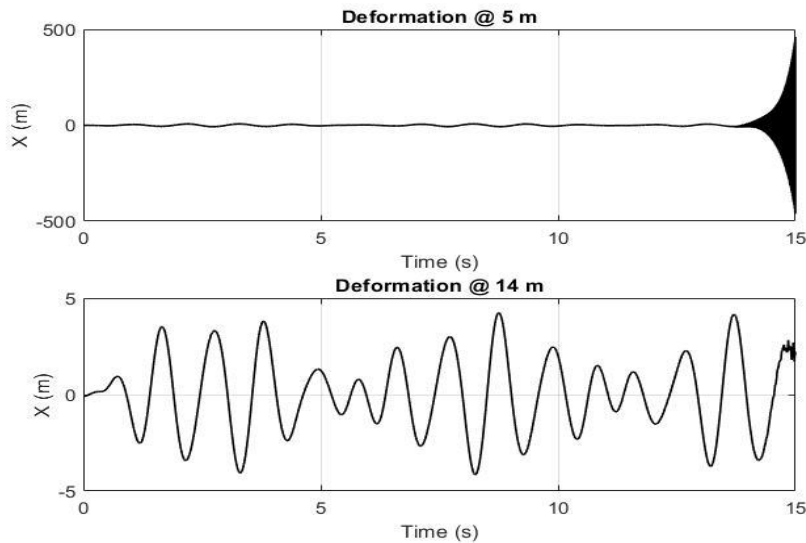


Figure 5-27 _ Vertical displacement with element length =5cm

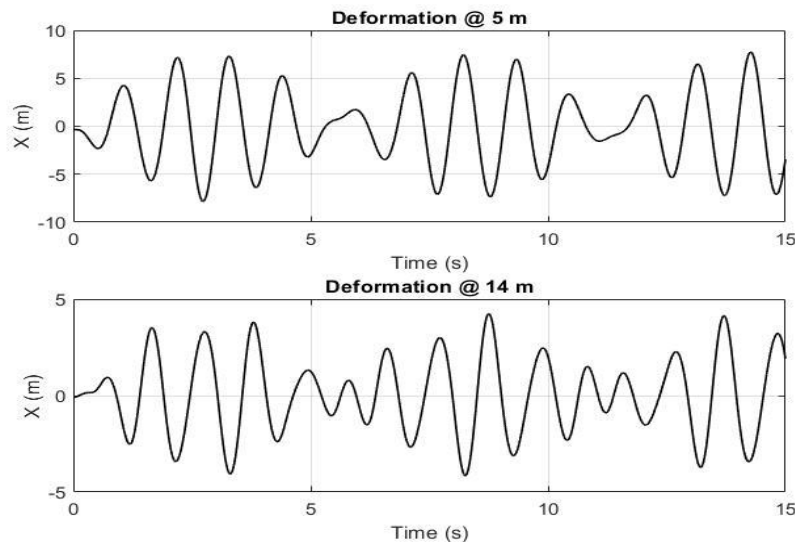


Figure 5-28 _ Vertical displacement, with element length =4.76cm

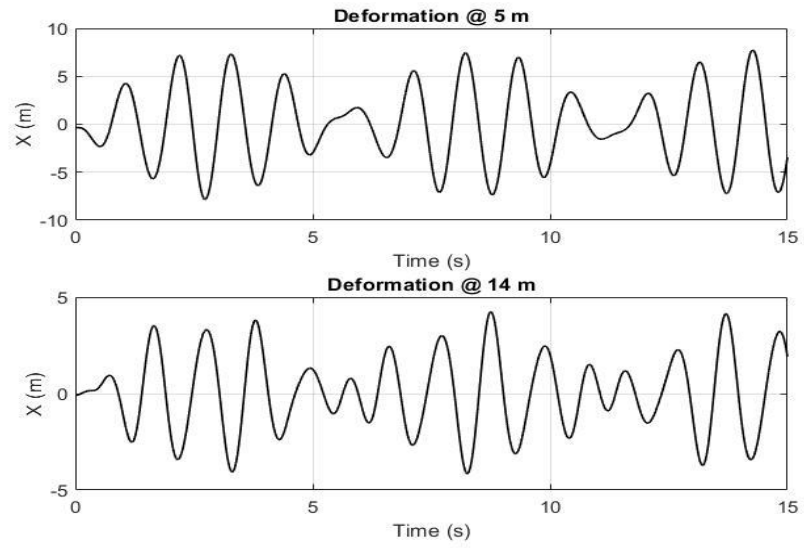


Figure 5-29 _ Vertical displacement, with element length =4.54cm

6 3rd Configuration: Multi-Span beam carrying multiple lumped elements and a lumped system

To prove the accuracy and reliability of our simulation, validation through a paper on “Journal of Sounds and Vibration”. (Lin, 2009) has been adopted.

This paper introduced a numerical assembly method (NAM) to find the correct values of natural frequencies and mode shapes of a multi-span Timoshenko beam. The mentioned beam carries multiple lumped elements and a seismic lumped system.

The configuration that is adopted to simulate and validate our work, is a pinned-pinned beam with an intermediate pin support which is depicted in figure 6.1.

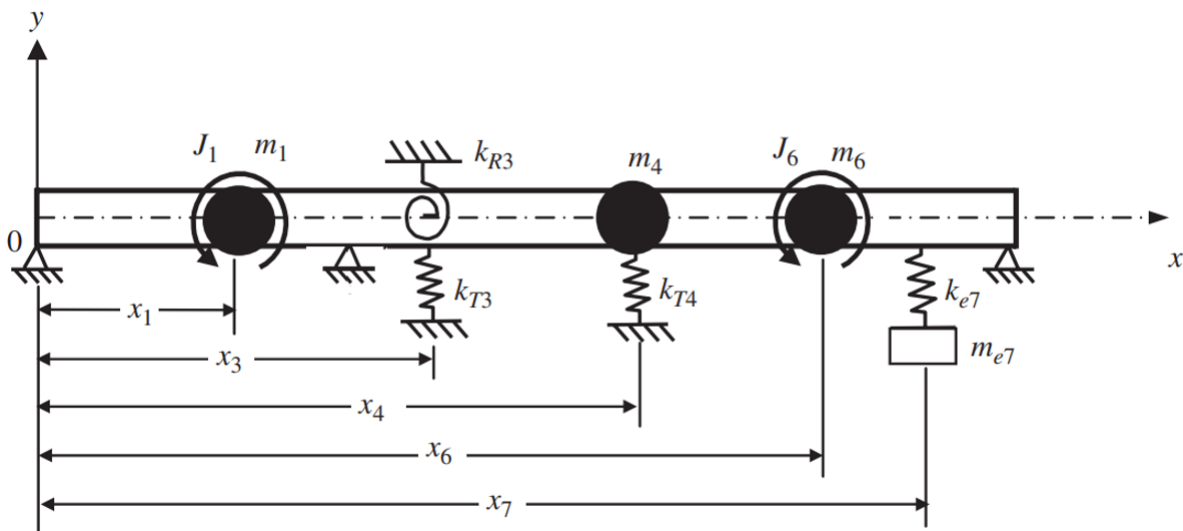


Figure 6-1 _ Sketch for a uniform Euler-Bernoulli beam supported by one intermediate pin, carrying a spring-mass system and number of various lumped elements

Table 6.1 _ Geometric data and parameters of the system

Density ρ	$7.835e^3 \frac{kg}{m^3}$	Rectangular cross section
Elastic modulus E	$2.069e^{11} N/m^2$	Width b_l $5e^{-2} m$
Shear coefficient k'	$5/6$	Height h_l $6e^{-2} m$
Poisson ratio ν	0.3	length l 1 m
Shear modulus G	$7.9577e^{10} N/m^2$	

All the elements and their corresponding values are expressed in table 6.2

Table 6.2 _ Elements' values

	m_1 (kg)	m_4 (kg)	m_6 (kg)	J_1 (kgm ²)	J_6 (kgm ²)	k_{T3} $(\frac{N}{m})$	k_{T4} $(\frac{N}{m})$	k_{R3} (Nm)	m_{e7} (kg)	k_{e7} $(\frac{N}{m})$
	4.701	4.701	9.402	0.04701	0.14103	$1.86210e^6$	$2.79315e^6$	$9.3105e^5$	4.701	$5.5863e^5$
location	x_1	x_4	x_6	x_1	x_6	x_3	x_4	x_3	x_7	x_7

And $x_1 = 0.2m$, $x_3 = 0.4m$, $x_4 = 0.6m$, $x_6 = 0.8m$, $x_7 = 0.9m$.

6.1 Introducing lumped elements to the system

To introduce the elements, the same approach which has been used to introduce constraints, is adopted, but this time since there are masses and inertias, since they are associated with the kinetic energy, their presence in the system lead to the increment in kinetic energy:

Incrementation of kinetic energy (ΔT) in correspondence of, lumped mass m_1 and lumped inertia J_1 is, as a matter of example:

$$\Delta T_{m_1} = \frac{1}{2}m_1(\dot{u}_{x_{x_1}})^2 + \frac{1}{2}m_1(\dot{u}_{y_{x_1}})^2 + \frac{1}{2}m_1(\dot{u}_{z_{x_1}})^2$$

$$\Delta T_{J_1} = \frac{1}{2}J_1(\dot{\theta}_{x_{x_1}})^2 + \frac{1}{2}J_1(\dot{\theta}_{y_{x_1}})^2 + \frac{1}{2}J_1(\dot{\theta}_{z_{x_1}})^2$$

In which the indices x_1 below each DOF, indicates that the degree of freedom is associated with node located at $x = x_1$.

Then:

$$\frac{d}{dt} \left(\frac{\partial \Delta T_{m_1}}{\partial \dot{u}_{x_{x_1}}} \right) = m_1 \dot{u}_{x_{x_1}} \qquad \frac{d}{dt} \left(\frac{\partial \Delta T_{J_1}}{\partial \dot{\theta}_{x_{x_1}}} \right) = J_1 \dot{\theta}_{x_{x_1}}$$

$$\frac{d}{dt} \left(\frac{\partial \Delta T_{m_1}}{\partial \dot{u}_{y_{x_1}}} \right) = m_1 \dot{u}_{y_{x_1}} \qquad \frac{d}{dt} \left(\frac{\partial \Delta T_{J_1}}{\partial \dot{\theta}_{y_{x_1}}} \right) = J_1 \dot{\theta}_{y_{x_1}}$$

$$\frac{d}{dt} \left(\frac{\partial \Delta T_{m_1}}{\partial \dot{u}_{z_{x_1}}} \right) = m_1 \dot{u}_{z_{x_1}} \qquad \frac{d}{dt} \left(\frac{\partial \Delta T_{J_1}}{\partial \dot{\theta}_{z_{x_1}}} \right) = J_1 \dot{\theta}_{z_{x_1}}$$

Then, in the global mass matrix of the system, the value m_1 will be added to every translational DOFs associated with that node where m_1 is added, and in the same way, the value J_1 will be added to every rotational DOFs associated with node on which J_1 is added.

6.2 Introducing lumped system (dynamic shock absorber) to the system

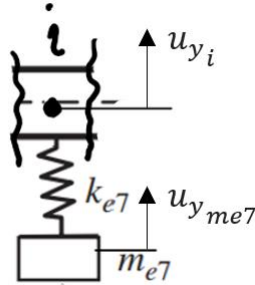


Figure 6-2 _ The seismic system attached to the beam at node i

According to figure 6.2, the seismic system adds an additional degree of freedom ($u_{y_{me7}}$) to the node to which it is attached. In order to introduce the spring-mass system to the global mass and stiffness matrices, initially this DOF is added to global displacement vector and, by following similar procedure, the correspondence elements of matrices will be obtained:

$$\Delta T_{m_{e7}} = \frac{1}{2} m_{e7} (\dot{u}_{y_i} - \dot{u}_{y_{me7}})^2$$

$$\Delta U_{k_{e7}} = \frac{1}{2} k_{e7} (u_{y_i} - u_{y_{me7}})^2$$

$$\frac{d}{dt} \left(\frac{\partial \Delta T_{m_{e7}}}{\partial \dot{u}_{y_i}} \right) = m_{e7} (\dot{u}_{y_i} - \dot{u}_{y_{me7}})$$

$$\frac{d}{dt} \left(\frac{\partial \Delta U_{k_{e7}}}{\partial u_{y_i}} \right) = k_{e7} (u_{y_i} - u_{y_{me7}})$$

$$\frac{d}{dt} \left(\frac{\partial \Delta T_{m_{e7}}}{\partial \dot{u}_{y_{me7}}} \right) = m_{e7} (-\dot{u}_{y_i} + \dot{u}_{y_{me7}})$$

$$\frac{d}{dt} \left(\frac{\partial \Delta U_{k_{e7}}}{\partial u_{y_{me7}}} \right) = k_{e7} (-u_{y_i} + u_{y_{me7}})$$

To the stiffness matrix, the additional elements are introduced as it follows:

$$\begin{bmatrix} \vdots & \vdots & \vdots & \vdots & \vdots \\ \cdots & \blacksquare + k_{e7} & \cdots & 0 - k_{e7} & \cdots \\ \vdots & \vdots & \ddots & \vdots & \vdots \\ \cdots & 0 - k_{e7} & \cdots & 0 + k_{e7} & \cdots \\ \vdots & \vdots & \vdots & \vdots & \vdots \end{bmatrix} \begin{Bmatrix} \vdots \\ u_{y_i} \\ \vdots \\ u_{y_{me7}} \\ \vdots \end{Bmatrix}$$

With respect to the mass matrix:

$$\begin{bmatrix} \vdots & \vdots & \vdots & \vdots & \vdots \\ \cdots & \blacksquare + m_{e7} & \cdots & 0 - m_{e7} & \cdots \\ \vdots & \vdots & \ddots & \vdots & \vdots \\ \cdots & 0 - m_{e7} & \cdots & 0 + m_{e7} & \cdots \\ \vdots & \vdots & \vdots & \vdots & \vdots \end{bmatrix} \begin{Bmatrix} \vdots \\ u_{y_i} \\ \vdots \\ u_{y_{me7}} \\ \vdots \end{Bmatrix}$$

6.3 Results

The results obtained are close to those presented in the paper. In the following figure 6.3, are depicted the first five modes from the paper for a Timoshenko beam, whilst figure 6.4, presents the corresponding results of our simulation:

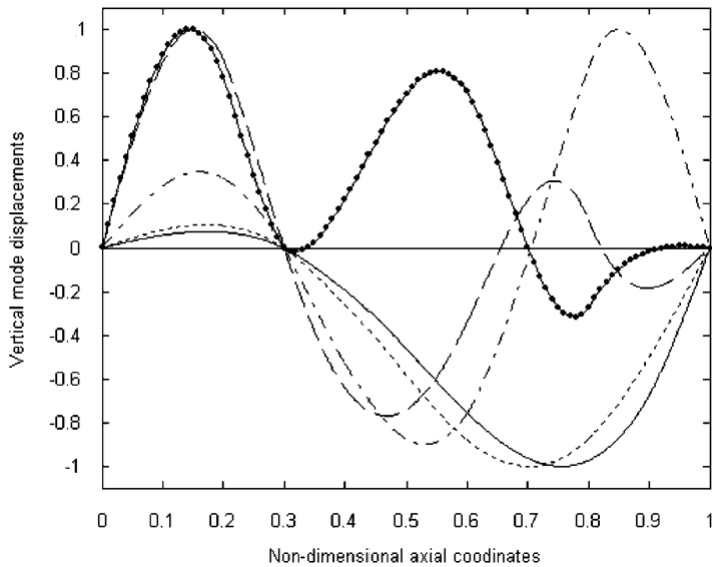


Figure 6-3 _ The lowest five mode shapes of the two-span pinned–pinned (P–P) Timoshenko beam

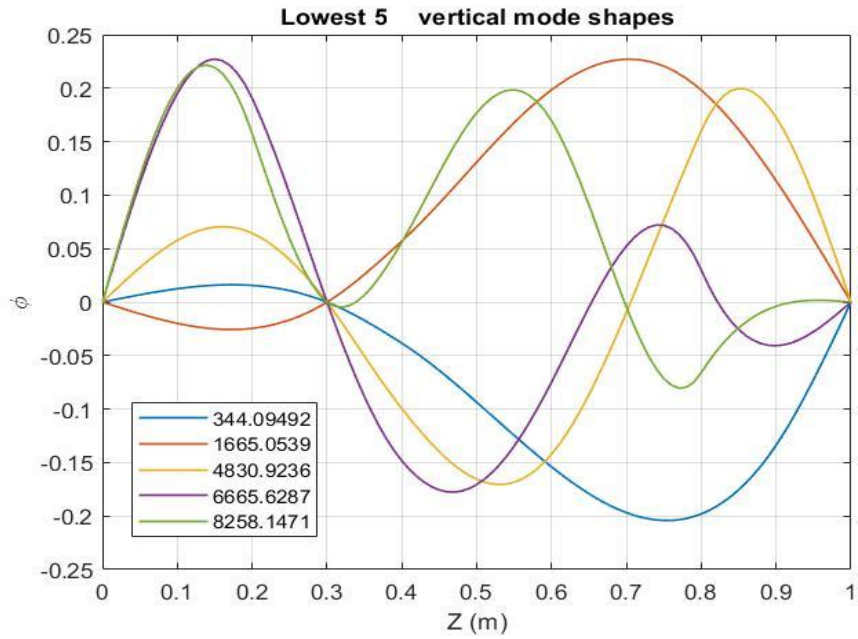


Figure 6-4 The lowest five modals of two-span Euler-Bernoulli beam carrying multiple lumped elements

Table 6.3 The lowest five natural frequencies of the two-span beam

Type of beam	Methods	ω_1 (rad/s)	ω_2 (rad/s)	ω_3 (rad/s)	ω_4 (rad/s)	ω_5 (rad/s)
Timoshenko beam	(NAM) paper	344.0505	1630.4214	4666.1223	6410.2455	7724.3333
Euler-Bernoulli beam	(NAM) paper	344.0948	1667.1936	4849.1637	6700.1525	8301.3915
Euler-Bernoulli beam	Present work	344.09492	1665.0539	4830.9236	6665.6287	8258.14171

7 Conclusion

The dynamic behavior of a single rope cable car under different load conditions in three-dimension has been analyzed in this thesis work. Due to the high complexity of the entire multi-span cable car structure under different conditions, it was necessary to implement a finite element method to consider different aspects of the operating system. According to previous works (Strauss, 2014), and various approaches which have been adopted to validate our FE-MATLAB code, the efficiency, and reliability of an Euler-Bernoulli beam element-based model has been proven with satisfactory consistency of the outcomes. On the other side, discretizing the model in time and utilizing the Newmark scheme as an approach to time integration has shown strong reliability and performance.

Considering that a beam under tensile load would cause geometry nonlinearity to our equations, in order to prevent nonlinearity, the formula (3.9) has been adopted, which based on some assumption linearizing the equation and introducing the additional bending stiffness due to that pretension. All the simulations with respect to a taut single-span cable appeared convincing and acceptable. When moving from a single-span cable to a longer cable passing through multi suspension towers, a longer cable under the same tensile load, the results of such a configuration were not correct.

In process of validating our simulation, according to the modal analysis of a multi-span beam carrying multiple lumped elements and system without any pretension in chapter 6, the validation came up with strong proof that the Euler-Bernoulli based model, which has been developed so far, was still trustworthy. Even the same outcomes were achieved when a similar configuration of two-span cable without pretension was modeled in some other commercial FEM software.

Furthermore, it has been shown that under tensile load, by increasing the radius of the cross-section of the cable and/or decreasing the length of the cable, the result of the pre-tensioned cable becomes more rational and closer to our expectations. As a result, the idea that the cable being too much long and very slender may violate the assumption based on which the linearization of formula (3.9) was carried out and the result are diverging from the correct ones is concluded. Otherwise, all results correspond to multi-span cable without pretension were satisfactory, and this inconsistency arises only in the case of very long pre-tensioned multi-span cable.

Acknowledgement

First and foremost, I am extremely grateful to my supervisor, Prof. Luigi Garibaldi for believing in me and providing me with this great opportunity to work under his supervision at DIRG research group. His invaluable advice, continuous support, and patience during my thesis, helped me to pass all the ups and downs in the way to finalize this work. Moreover, I would like to express my deepest gratitude to him for the inspiration and all the supports he has provided me in the path of achieving a very exciting Ph.D position.

I would like to thank Prof. Alessandro Fasana for all the advice he has given to me and introducing me to Prof. Garibaldi. In addition, through his teachings and lectures I learned a lot and developed my interest in this field of study.

Last but not the least, I would like to thank my family and my friends for always supporting and encouraging me with their best wishes.

List of figures

Figure 2-1	_ Gondola lift	4
Figure 2-2	_ An illustrative 3D model of a gondola lift with two spans	5
Figure 2-3	_ Aerial Tramway	5
Figure 3-1	_ Beam element and reference frame.....	9
Figure 3-2	_ Euler-Bernoulli beam element and axial degrees of freedom.....	12
Figure 3-3	_ Euler-Bernoulli beam element and torsional degrees of freedom.....	13
Figure 3-4	_ Euler-Bernoulli beam element and flexural degrees of freedom within xz plane.....	15
Figure 3-5	_ Euler-Bernoulli beam element and flexural degrees of freedom within yz plane.....	19
Figure 3-6	_ Euler-Bernoulli beam element with axial force T.....	21
Figure 3-7	_ Flowchart – Newmark integration for linear systems	24
Figure 4-1	_ General E-B beam element with local and global reference frame respectively O and O' ..	25
Figure 4-2	_ single-span cable modelled as a beam of N E-B elements.....	29
Figure 4-3	_ Total stiffness matrix of the structure configuration.....	31
Figure 4-4	_ Static deformation	35
Figure 4-5	_ 1st vertical mode shape	38
Figure 4-6	_ 2nd vertical mode shape.....	38
Figure 4-7	_ 3rd vertical mode shape	38
Figure 4-8	_ 4th vertical mode shape.....	38
Figure 4-9	_ 5th vertical mode shape.....	38
Figure 4-10	_ The first five modes in lateral direction	39
Figure 4-11	_ The response of the system to step function respectively at $z = 2\text{m}$ and $z = 4\text{m}$	42
Figure 4-12	_ The vertical reaction forces of the constraints	42
Figure 4-13	_ Harmonic response of the system at two points.....	44
Figure 4-14	_ The vertical reaction forces of the constraints due to harmonic excitation.....	44
Figure 4-15	_ Scheme of the system under analysis.....	45
Figure 4-16	_ Time history of displacement at two points	46
Figure 4-17	_ Deformation of the cable in the position under the load.....	47
Figure 4-18	_ The variation of the vertical reaction forces over time	47
Figure 5-1	_ General orientation of beam in space.....	49
Figure 5-2	_ Two-span beam with one intermediate constraint	52
Figure 5-3	_ Static equilibrium.....	55
Figure 5-4	_ The 1st vertical mode, $T = 0$	57
Figure 5-5	_ The 2nd vertical mode, $T = 0$	57
Figure 5-6	_ The 3rd vertical mode, $T=0$	57
Figure 5-7	_ The 4th vertical mode, $T=0$	57
Figure 5-8	_ The 5th vertical mode, $T=0$	57
Figure 5-9	_The first five modes in lateral direction.....	58
Figure 5-10	_ The 1st vertical mode, $T=20\text{kN}$	59
Figure 5-11	_ The 2nd vertical mode, $T=20\text{kN}$	59
Figure 5-12	_ The 3rd vertical mode, $T=20\text{kN}$	59
Figure 5-13	_ The 4th vertical mode, $T=20\text{kN}$	59

Figure 5-14 _ The 5th vertical mode, T=20kN	59
Figure 5-15 _ The 1st vertical mode, T=100kN	60
Figure 5-16 _ The 2nd vertical mode, T=100kN	60
Figure 5-17 _ The 3rd vertical mode, T=100kN	60
Figure 5-18 _ The 4th vertical mode, T=100kN	60
Figure 5-19 _ The 5th vertical mode, T=100kN	60
Figure 5-20 _ Step response of two nodes at 5m & 14m.....	63
Figure 5-21 _ Variation of reaction forces over time	63
Figure 5-22 _ Harmonic response of two nodes at 5m & 14m.....	64
Figure 5-23 _ Variation of reaction forces over time	65
Figure 5-24 _ Time history of displacement at two points	65
Figure 5-25 _ Deformation of the cable with correspondence of the load	66
Figure 5-26 _ The variation of the vertical reaction forces over time	66
Figure 5-27 _ Vertical displacement with element length =5cm.....	67
Figure 5-28 _ Vertical displacement, with element length =4.76cm.....	67
Figure 5-29 _ Vertical displacement, with element length =4.54cm.....	68
Figure 6-1 _ Sketch for a uniform Euler-Bernoulli beam supported by one intermediate pin, carrying a spring-mass system and number of various lumped elements	69
Figure 6-2 _ The seismic system attached to the beam at node i.....	72
Figure 6-3 _ The lowest five mode shapes of the two-span pinned-pinned (P-P) Timoshenko beam....	73
Figure 6-4 _ The lowest five modals of two-span Euler-Bernoulli beam carrying multiple lumped elements	74

List of tables

Table 4.1 _ Geometrical data and parameters of the system	25
Table 4.2 _ Assembling three elements of a single-span beam	30
Table 4.3 _ Natural frequency values (Hz).....	39
Table 5.1 _ Geometrical data and parameters of the system	49
Table 5.2 _ Assembling table.....	52
Table 5.3 _ Natural frequency values (Hz).....	58
Table 6.1 _ Geometric data and parameters of the system	70
Table 6.2 _ Elements' values.....	70
Table 6.3 _ The lowest five natural frequencies of the two-span beam	74

Bibliography

- A. Crotti, D. A. (A cura di). (2006). *Impianti a fune. Elementi costitutivi, progettazione ed esercizio*.
- Ambrósio, J. (2012). A COMPUTATIONAL PROCEDURE FOR THE DYNAMIC ANALYSIS OF THE CATENARY-PANTOGRAPH INTERACTION IN HIGH-SPEED TRAINS. *Journal of Theoretical and Applied Mechanics*.
- Anastasio, D. (2020 May 14). *Modeling and experimental identification of vibrating structures: localized and distributed nonlinearities*. Turin, Italy: Politecnico di Torino.
- B. Carboni, A. Arena, W. Lacarbonara. (2020). Nonlinear vibration absorbers for ropeway roller batteries control. *Journal of Mechanical Engineering Science*.
- Belluati, C. (2021). *Fenomeni oscillatori su impianti di trasporto bifune in esercizio: analisi dinamica e proposte per lo smorzamento*. Master thesis, Politecnico di Torino.
- BUSCEMI, M. (2016). *Studio di un sistema di controllo attivo per la riduzione delle vibrazioni nelle linee aeree di trasmissione dell'energia elettrica*. Politecnico di Milano.
- D. Anastasio, A. Fasana, L. Garibaldi, S. Marchesiello. (14 June 2018). Analytical investigation of railway overhead contact wire. *Mechanical Systems and Signal Processing*.
- G. Poetsch, J. Evans. (1997). Pantograph/Catenary Dynamics and Control. *Vehicle System Dynamics*.
- G.Genta. (2008). *Vibration dynamics and control*. Springer.
- H.Sugiyama & Ahmed A. Shabana. (2005). Three-Dimensional Large Deformation Analysis of the Multibody Pantograph/Catenary Systems. *Nonlinear Dynamics*.
- J. Benet et al. (2013). An advanced 3D-model for the study and simulation of the pantograph catenary system. *Transportation Research Part C: Emerging Technologies*.
- J.-H. Lee and T.-W. Park. (2012). Development of a three-dimensional catenary model using cable elements based on absolute nodal coordinate formulation. *Journal of mechanical science and technology*.
- J.Pombo, J.Ambrósio . (2012 b). Multiple Pantograph Interaction With Catenaries in High-Speed Trains. *J. Comput. Nonlinear Dynam.*
- J.Pombo, J.Ambrósio. (2012 a). Influence of pantograph suspension characteristics on the contact quality with the catenary for high speed trains. *Computers & Structures*.
- J.Pombo, J.Ambrosio. (2013). Environmental and track perturbations on multiple pantograph interaction with catenaries in highspeed trains. *Computers & Structures*.
- Joseph R.Rieker, Yih-HwangLin, Martin W.Trethewey. (2003). Discretization considerations in moving load finite element beam models. *Finite Elements in Analysis and Design*.
- K.Hoffmann, R.Petrova. (2009). Simulation of vortex excited vibrations of a bicable ropeway.

- Lin, H.-Y. (2009). On the natural frequencies and mode shapes of a multispan Timoshenko beam carrying a number of various concentrated elements. *JOURNAL OF*.
- M. Géradin, D. Rixen . (1997). *Mechanical vibrations*. John Wiley.
- Ning Zhou. (2011). Dynamic performance of a pantograph-catenary system with the consideration of the appearance characteristics of contact surfaces. *Journal of Zhejiang University*.
- O.Lopez-Garcia, A.Carniceroa, V.Torresb. (2006). Computation of the initial equilibrium of railway overheads based on the catenary equation. *Engineering Structures*.
- Onore, M. (2018). *Smorzatore Stockbridge e soppressione delle vibrazioni dei cavi tesi*:. Politecnico di Torino.
- R.Petrova, St.Karapetkov, S.Dechkova, Pl.Petrov. (2011). Mathematical Simulation of Cross-Wind Vibrations in a Mono-Cable Chair Ropeway. *ELSEVIER*.
- Rauter, F. G. (2007). Contact Model for The Pantograph-Catenary Interaction. *Journal of System Design and Dynamics*.
- Sciuto, G. (2015). *Application of innovative GNSS / INS techniques for the determination of dynamic behavior of cableways* . University of Trieste.
- Strauss, A. (2014). *Development of numerical models for the dynamic analysis of pantograph-catenary interaction*. Master thesis, Politecnico di Torino.
- Yong Hyeon Cho, Kiwon Lee. (2010). Influence of contact wire pre-sag on the dynamics of pantograph–railway catenary. *International Journal of Mechanical Sciences*.
- Zhou Yang, Xue-Ping Li, Jun Li, Tian-Sheng Hong, Kun-Peng Xue. (2015). Transversal Vibration of Chain Ropeway System Having Support Boundary Conditions with Polygonal Action. *Shock and Vibration*.